Dual Action Ru(II) Complexes With Bulky π-Expansive Ligands: Phototoxicy Without DNA Intercalation

Nicholas P. Toupin,[1†] Sandeep Nadella,[1†] Sean J. Steinke,[2] Claudia Turro,[2*]

Jeremy J. Kodanko[1,3*]

[1]Department of Chemistry, Wayne State University, 5101 Cass Ave, Detroit, MI 48202
[2]Department of Chemistry and Biochemistry, The Ohio State University, Columbus, OH 43210
[3]Barbara Ann Karmanos Cancer Institute, Detroit, MI 48201

[†]These authors contributed equally to this work

Abstract. We report the synthesis, photochemical, and biological characterization of Ru(II) complexes containing π-expansive ligands derived from dimethylbenzo[i]dipyrido[3,2-a:2',3'-c]phenazine (Me_2dppn) adorned with flanking aryl substituents. Late stage Suzuki couplings produced Me_2dppn ligands substituted at the 10 and 15 positions with phenyl (**5**), 2,4-dimethylphenyl (**6**) and 2,4-dimethoxyphenyl (**7**) groups. Complexes of the general formula $[Ru(tpy)(L)(py)](PF_6)_2$ (**8**–**10**), where L = **4**–**7**, were characterized and shown to have dual photochemotherapeutic (PCT) and photodynamic therapy (PDT) behavior. Quantum yields for photodissociation of monodentate pyridines from **8**–**10** were about 3 times higher than that of parent complex $[Ru(tpy)(Me_2dppn)(py)](PF_6)_2$ (**1**), whereas quantum yields for singlet oxygen ($^1O_2$) production were ~10% lower than that of **1**. Transient absorption spectroscopy indicates that **8**–**10** possess long excited state lifetimes (τ = 46–50 μs), consistent with efficient $^1O_2$ production through population and subsequent decay of ligand-centered $^3\pi\pi^*$ excited states. Complexes **8**–**10** displayed greater lipophilicity relative to **1** and association to DNA, but do not intercalate between the duplex base pairs. Complexes **1** and **8**–**10** showed photoactivated toxicity in breast and prostate

cancer cell lines with phototherapeutic indexes, PIs, as high as >56, where the majority of cell death was achieved 4 h after treatment with Ru(II) complexes and light. Flow cytometric data and rescue experiments were consistent with necrotic cell death mediated by the production of reactive oxygen species, especially $^1O_2$. Collectively, this study confirms that DNA intercalation by Ru(II) complexes with π-expansive ligands is not required to achieve photoactivated cell death.

Introduction

Ruthenium complexes have broad applications in solar energy capture, photocaging, photodynamic therapy (PDT), and photochemotherapy (PCT).[1-4] For biological applications including PDT and PCT, Ru(II) complexes show many attractive properties, including cell permeability,[5,6] low inherent toxicity,[7-10] efficient photodissociation of ligands,[11-19] and high dark to light ratios for cancer cell death.[20-24] Long-standing efforts in the development of Ru(II)-based photosensitizers have led to recent success in the achievement of a major milestone. The compound TLD-1433, which is first Ru(II)-based photosensitizer to enter the clinic, advanced to Phase II clinical trials for the treatment of non-muscle invasive bladder cancer due to promising results in preclinical development and earlier trials.[25]

An important feature of Ru(II) complexes is that they absorb visible light strongly into singlet metal-to-ligand charge transfer (^{1}MLCT) states that undergo intersystem crossing with nearly 100% yield to populate corresponding triplet MLCT (^{3}MLCT) states.[26] Coordination of a ligand with an extended π-system that possesses a ligand-centered $^3\pi\pi^*$ state that falls below the ^{3}MLCT state results in long excited state lifetimes (20–50 μs) that efficiently produce singlet oxygen ($^1O_2$),[27] the mechanism of action for most Type II photosensitizers used in clinical PDT.[28] In addition, complexes with sterically encumbered ligands that distort the coordination around the

Ru(II) center from the ideal octahedral geometry results in lower energy metal-centered state(s) of anti-bonding character that can be populated from ^{3}MLCT states, which facilitates ligand dissociation, the concept exploited in PCT.[15,29] The Turro laboratory was the first to report Ru(II)-based complexes that show dual activity accessible with low energy light, resulting in both the photosensitized production of $^1O_2$ and the photodissociation of aromatic heterocycles as models for drug molecules (Figure 1).[15,27] The π-expansive ligand 3,6-dimethylbenzo[i]dipyrido[3,2-a:2',3'-c]phenazine (Me_2dppn) contains a phenanthroline core fused with a diaminonaphthalene unit and was an essential component of this dual-action PDT/PCT agent. Importantly, the combination of PCT and PDT realized with a Me_2dppn-containing Ru(II) complex was shown to be critical for achieving efficient, light-activated cell death in *in vitro* models of triple-negative breast cancer.[30] Related complexes that underwent either PCT or PDT alone showed minimal, if any, cytotoxicity in these 2D and 3D culture models, proving that dual action PCT/PDT creates and promotes efficacy of Ru(II) compounds against cancer cells.

Figure 1. Schematic representation of the molecular structure of dual action Ru(II) complex **1** containing the ligand Me_2dppn and its photoactivated ligand dissociation for PCT and $^1O_2$ photosensitization for PDT.

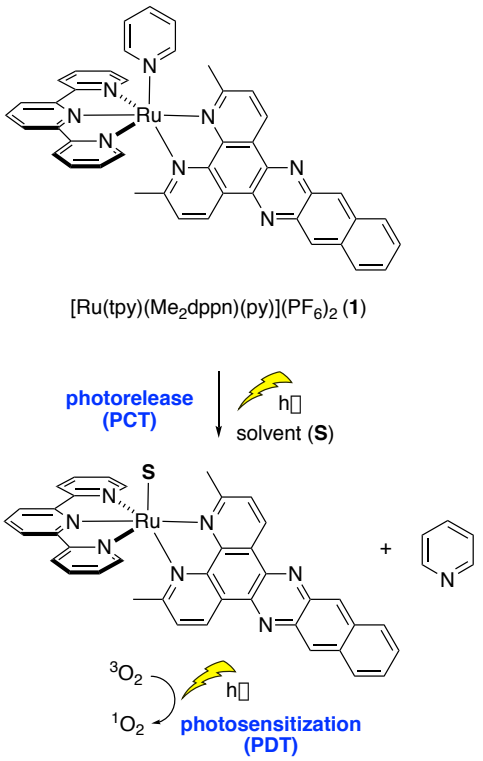

Aside from dual-action PCT/PDT agents, derivatives of the ligand dppn (Figure 2) have been incorporated into Ru(II) and related metal complexes for research in photochemistry, solar energy capture,[31] sensing,[32] and biology, including anticancer[20,33-35] and antibacterial[36,37] applications, amongst other work not cited here. Derivatives of dppn are underexplored, as opposed to other π-expansive ligands such as 3,6-dimethyldipyrido[3,2-a:2',3'-c]phenazine (dppz, Figure 2); a SciFinder search shows >100 analogs of dppz have been reported. Derivatives of dppn include structures shown in Figure 2. Analogs with substituents at the 3- (pydppn),[38-41] 3- and 6-

(Me_2dppn, Bu_2dppn)[42] and 10- and 15-positions (Br_2dppn[43] and (i-$Pr_3SiCC)_2$dppn[44]) have been synthesized. In addition, the *p*-quinone analog qdppn has been incorporated into several Ru(II) complexes with short-lived excited states that show low yields for $^1O_2$ generation.[20,45] The tetrathiafulvalene ligand exTTF-dpq was built into the complex $[Ru(bpy)_2(exTTF\text{-}dpq)]^{2+}$, which shows absorbance at > 650 nm that is red-shifted by ~100 nm compared with $[Ru(bpy)_2(qdppn)]^{2+}$.[46] Other derivatives include the pyrene-containing ligand pyrene-phen[47] and the carboxylic acid analog dppbz.[48]

A major theme for Ru(II) complexes derived from dppn is their ability to bind, intercalate, and photocleave DNA. In some cases, the extended π-system of dppn may provide stronger binding and intercalation of Ru(II) complexes with DNA than complexes derived from dppz.[49,50] Photocleavage of purified DNA by dppn-containing Ru(II) complexes has been demonstrated owing to its efficient production of $^1O_2$ from a dppn-centered $^3\pi\pi^*$ state, combined with its strong DNA binding.[51,52] The complexes $[Ru(tpy)(pydppn)]^{2+}$ and $[Ru(pydppn)_2]^{2+}$ generated photodynamic DNA-protein and protein crosslinks in human fibroblasts, including p53 and proliferating cell nuclear antigen (PCNA) crosslinks, consistent with nuclear targeting and DNA oxidation.[39] In this case, data indicated that oxidative crosslinking was due to generation of $^1O_2$ because crosslinking could be blocked by pretreatment of the cells with sodium azide, an efficient $^1O_2$ scavenger. Although most studies implicate DNA targeting, other work suggests that dppn-containing Ru(II) complexes may interact with the cell membrane and lipid bilayers in cells.[53,54] In general, it is often assumed that complexes of this class target and intercalate DNA in cells, but research that probes the mechanism of cell death using cell-based assays has been limited.[39,54]

In this manuscript, we describe the synthesis, characterization, and the photochemical and biological properties of Ru(II) complexes containing arylated derivatives of the ligand Me_2dppn

that were designed to increase lipophilicity and to block DNA intercalation. We report a late-stage divergent approach for the synthesis of Me_2dppn analogs that provides rapid access to new Me_2dppn ligands with aryl substituents attached to the 10- and 15 positions. Despite the fact that these new Ru(II) complexes are not expected to intercalate between the DNA bases, herein we show that they interact with DNA and exhibit dual action PCT/PDT activity, with photoactivated toxicity in breast and prostate cancer cells that is achieved on short timescales. Investigations into the mode of cell death by Ru(II) complexes containing Me_2dppn and its analogs indicate that high phototherapeutic indexes (PIs) can be achieved, and that rapid cellular necrosis, rather than apoptosis, is the dominant mechanism of death at early time points. This work shows that cell death can be rescued using scavengers of reactive oxygen species (ROS), consistent with ROS generation, especially $^1O_2$, being responsible for the cytotoxicity of these compounds and is important for future design of dual-action PDT/PCT complexes.

Figure 2. Bidentate π-expansive ligands include dppz and dppn derivatives

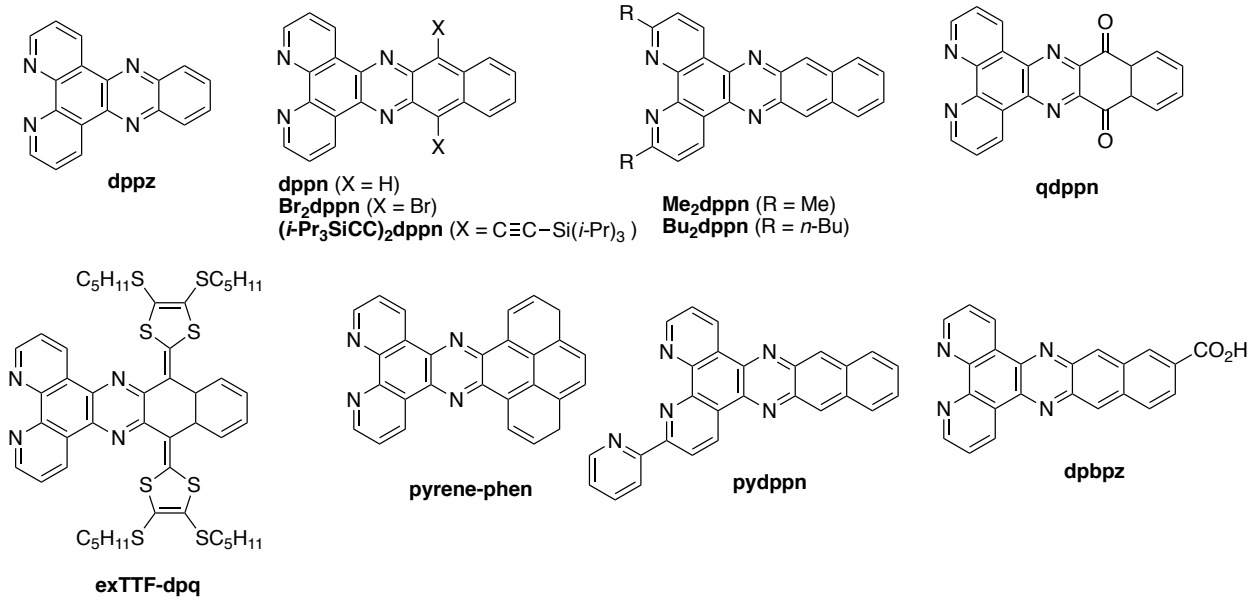

Experimental Section

General Considerations

NMR and IR spectral data and mass spectrometry data were collected as previously described.[30] Reactions were performed under ambient atmosphere unless otherwise noted.

Instrumentation

Steady state electronic absorbance spectra were collected using an Agilent Cary 8454 diode array spectrophotometer or Agilent Technologies Cary-Win UV-vis spectrometer. Emission data were collected using a Horiba FluoroMax-4 fluorimeter. The irradiation source for quantum yield measurements was a 150 W Xe arc lamp (USHIO) in a MilliArc lamp housing unit, powered by a LPS-220 power supply and aLPS-221 igniter (PTI). Irradiation wavelengths for steady-state photolysis were controlled with long-pass filters (CVI Melles Griot) and quantum yield experiments were conducted using a 500 nm bandpass filter (Thorlabs). Relative viscosity measurements were performed using a Cannon-Manning semi-micro viscometer for transparent liquids submerged in a water bath maintained at 25 °C by a Neslab model RGE-100 circulator. Nanosecond transient absorption was performed using a LP980, Edinburgh Instruments spectrometer equipped with a 150 W Xe arc lamp (USHIO) as the probe beam, an intensified CCD (ICCD) detector and a PMT. The samples were excited by the output of an optical parametric oscillator (basiScan, Spectra-Physics) pumped by a Nd:YAG laser (Quana-Ray INDI, Spectra-Physics) as an excitation source with fwhm = 8 ns. The spectra were collected at various time details with an ICCD camera, and kinetic traces were recorded using a PMT and digital oscilloscope.

Methods

The quantum yields for photoinduced ligand exchange in **8**–**10** were measured at λ_{irr} = 500 nm in MeCN using potassium ferrioxalate as an actinometer following a previously published procedure.[55] Singlet oxygen quantum yields were performed using $[Ru(bpy)_3]^{2+}$ as a standard (Φ_Δ = 0.81 in MeOH), 1,3-diphenylisobenzofuran (DPBF) as a $^1O_2$ trapping agent, and following previously established procedure.[56] Steady-state and time-resolved electronic absorption was performed using 1 x 1 cm quartz cuvettes and the concentration of samples for transient absorption spectroscopy were adjusted to obtain an absorbance value of 0.5 at the excitation wavelength.

Relative viscosity and electronic absorption titrations were performed using calf thymus DNA purified overnight by dialysis against 5 mM Tris, 50 mM NaCl, pH 7.0 buffer. Changes to the electronic absorption spectra of 5 μM of **8** and **9** and 10 μM of **10** upon addition of increasing amounts of DNA (0–350 μM) in a manner not to affect the absorption by sample dilution were attempted to determine binding constants, K_b (5 mM Tris, 50 mM NaCl, pH 7.0), as is typical for complexes with extended π-systems.[57] However, self-aggregation of the complexes, enhanced aggregation in the presence of polyanionic DNA or polystyrene sulfonate (PSS), and interactions with hydrophobic DNA regions result in similar spectral changes, such that the accurate determination of K_b was not possible using this method.[58] Relative viscosity measurements were performed using sonicated calf thymus DNA that was an average length of ~200 base pairs in order to minimize DNA flexibility.[59] For these experiments, the ratio of the amount of metal complex or ethidium bromide to that DNA was increased by adding small volumes of concentrated stock solutions to the DNA sample already in the viscometer. Solutions in the viscometer were mixed by bubbling with nitrogen and equilibrated to 25 °C by allowing samples to equilibrate in the water

bath for 30 minutes prior to each measurement. Relative viscosities for DNA in the presence or absence of complex were calculated from eq 1,

$$\eta = \frac{(t-t_0)}{t_0} \quad (1)$$

where t is the flow time of a given solution containing DNA and t_0 is the flow time of buffer alone. Relative viscosity data are plotted as $(\eta/\eta_0)^{1/3}$ as a function of the ratio of complex to DNA concentration, where η is the relative viscosity of a solution at a given [Complex]:[DNA] ratio, and η_0 is the relative viscosity of a solution containing only DNA.

10,15-dibromo-3,6-dimethylbenzo[*i*]dipyrido[3,2-*a*:2',3'-*c*]phenazine (**Me_2Br_2dppn, 4**). 2,9-dimethyl-1,10-phenanthroline-5,6-dione[60] (0.55 g, 2.3 mmol) and 1,4-dibromo-2,3-diaminonaphthalene[61] (0.73 g, 2.3 mmol) were refluxed in EtOH (46 mL) at 80°C for 16 h under nitrogen atmosphere, during which time a red precipitate formed. The reaction mixture was cooled to room temperature and the precipitate was collected by filtration, then washed with EtOH and dried *in vacuo* to give **3** as a red solid (0.80 g, 1.5 mmol, 67%): ^{1}H NMR (400 MHz, $CDCl_3$) δ 9.61 (d, J = 8.2 Hz, 2H), 8.74 (dd, J = 6.9, 3.2 Hz, 2H), 7.75 (dd, J = 6.9, 3.3 Hz, 2H), 7.70 (d, J = 8.2 Hz, 2H), 3.04 (s, 6H); ^{13}C NMR (100 MHz, $CDCl_3$) δ 162.80, 136.49, 135.83, 134.82, 133.30, 128.74, 128.39, 125.53, 124.90, 124.24, 25.63; IR (KBr) 3059, 2978, 2954, 2916, 2360, 2342, 1672, 1618, 1582, 1463, 1420, 1378, 1260, 1130, 938, 832, 749; ESMS calculated for $C_{24}H_{15}Br_2N_4$ $[M+H]^+$: 517.0, found 516.9.

General Procedure for Suzuki Cross Coupling Reactions. Me_2Br_2dppn (**4**), aryl boronic acid, $PdCl_2$, PPh_3 and K_2CO_3 were combined in a sealable pressure tube. Water (4 mL), ethanol (6 mL) and toluene (8 mL) were added and the mixture was deoxygenated by bubbling Ar through a

submerged needle for 20 min. The pressure tube was sealed and the mixture was heated to reflux for 24 h. After aqueous workup, the crude product was purified via recrystallization or by chromatography on neutral alumina.

3,6-dimethyl-10,15-diphenylbenzo[*i*]dipyrido[3,2-*a*:2',3'-*c*]phenazine (Me_2Ph_2dppn, 5). Compound **5** was prepared using the general procedure for Suzuki cross coupling reactions from **4** (207 mg, 0.400 mmol), phenylboronic acid (148 mg, 1.21 mmol), $PdCl_2$ (7 mg, 0.04 mmol), PPh_3 (21 mg, 0.080 mmol) and K_2CO_3 (221 mg, 1.60 mmol). The reaction mixture was cooled to rt, diluted with ethyl acetate (10 mL) and washed with a saturated solution of aqueous $NaHCO_3$ (3 × 10 mL). The organic layer was separated, dried with anhydrous Na_2SO_4, filtered and concentrated. The crude product was recrystallized from hot EtOH to give **5** (117 mg, 0.228 mmol, 57%) as an orange solid. ^{1}H NMR (400 MHz, $CDCl_3$) δ 8.98 (dd, J = 8.1, 1.2 Hz, 2H), 8.18 – 8.13 (m, 2H), 7.73 – 7.62 (m, 10H), 7.52 (dt, J = 8.2, 1.3 Hz, 4H), 2.95 (s, 6H); ^{13}C NMR (100 MHz, $CDCl_3$) δ 161.5, 136.6, 133.8, 131.8, 131.6, 127.1, 126.8, 126.8, 125.8, 125.1, 123.8, 25.0; IR (KBr) 3048, 3030, 2965, 2919, 2870, 2823, 2723, 2357, 2339, 1587, 1487, 1439, 1395, 1364, 1348, 1101, 1070, 983, 953, 889, 833, 751, 702; ESMS calculated for $C_{36}H_{25}N_4$ $[M+H]^+$ 513.2, found 513.2.

10,15-bis(2,4-dimethylphenyl)-3,6-dimethylbenzo[*i*]dipyrido[3,2-*a*:2',3'-*c*]phenazine (Me_2(2,4-Me_2Ph_2)dppn, 6). Compound **6** was prepared using the general procedure for Suzuki cross coupling reactions from **4** (204 mg, 0.394 mmol), 2,4-dimethyl phenyl boronic acid (150 mg, 1.00 mmol), $PdCl_2$ (7 mg, 0.04 mmol), PPh_3 (21 mg, 0.080 mmol) and K_2CO_3 (221 mg, 1.60 mmol). The reaction mixture was cooled to rt, diluted with ethyl acetate (10 mL) and washed with a saturated solution of aqueous $NaHCO_3$ (3 × 10 mL). The organic layer was separated, dried with anhydrous Na_2SO_4, filtered and concentrated. The crude product was purified by column

chromatography on neutral alumina (7% EtOAc:hexanes) to give the pure compound **6** (124 mg, 0.217 mmol, 55%) as an orange solid. ^{1}H NMR (400 MHz, $CDCl_3$) δ 8.95 (d, *J* = 8.2 Hz, 2H), 7.89 (dt, *J* = 6.2, 3.0 Hz, 2H), 7.55 – 7.43 (m, 4H), 7.35 – 7.22 (m, 6H), 2.91 (s, 6H), 2.58 (s, 6H), 1.98 (d, *J* = 3.4 Hz, 6H); ^{13}C NMR (100 MHz, $CDCl_3$) δ 161.3, 147.4, 140.4, 137.4, 136.5, 135.9, 133.6, 133.5, 132.1, 130.9, 130.9, 129.8, 129.7, 126.7, 125.7, 125.2, 125.1, 123.8, 25.0, 20.7, 19.8; IR (KBr) 3064, 2996, 2948, 2919, 2855, 2728, 2363, 2343, 1684, 1612, 1587, 1542, 1507, 1489, 1458, 1425, 1364, 1348, 1301, 1201, 1180, 1130, 1122, 1072, 1033, 982, 956, 812, 766, 752, 722, 689, 638; ESMS calculated for $C_{40}H_{33}N_4$ $[M+H]^+$ 569.3, found 569.3.

10,15-bis(2,4-dimethoxyphenyl)-3,6-dimethylbenzo[*i*]dipyrido[3,2-*a*:2',3'-*c*]phenazine (Me$_2$(2,4-(MeO)$_2$Ph$_2$)dppn, 7). Compound **7** was prepared using the general procedure for Suzuki cross coupling reactions from **4** (208 mg, 0.401 mmol), 2,4-dimethoxy phenyl boronic acid (182 mg, 1 mmol), $PdCl_2$ (7 mg, 0.04 mmol), PPh_3 (21 mg, 0.080 mmol) and K_2CO_3 (221 mg, 1.60 mmol) are added to a pressure tube. Water (4 mL), ethanol (6 mL), toluene (8 mL) are added, argon gas is purged. After cooling to rt, the reaction mixture was diluted with CH_2Cl_2 (12 mL) and washed with a saturated solution of aqueous $NaHCO_3$ (3 × 12 mL). The organic layer was separated, dried with anhydrous Na_2SO_4, filtered and concentrated. The crude product was extracted by stirring with EtOAc:hexanes (10 mL, 1:1) for 3 h to give **7** (142 mg, 56%) as an orange solid. ^{1}H NMR (400 MHz, $CDCl_3$) δ 9.01 (d, *J* = 8.1 Hz, 2H), 8.02 (dd, *J* = 6.9, 3.3 Hz, 2H), 7.54 – 7.34 (m, 6H), 6.81 (ddt, *J* = 13.6, 5.5, 2.4 Hz, 4H), 4.03 (s, 6H), 3.64 (d, *J* = 5.3 Hz, 6H), 2.92 (s, 6H); ^{13}C NMR (100 MHz, $CDCl_3$) δ 161.60, 161.29, 160.93, 159.31, 159.26, 133.80, 127.63, 127.53, 126.45, 124.84, 104.20, 104.14, 99.58, 98.79, 77.32, 77.00, 76.68, 55.67, 55.57, 29.69; IR (KBr) 3065, 3034, 2998, 2951, 2934, 2834, 2361, 2342, 2332, 1608, 1581, 1509, 1458,

1436, 1364, 1349, 1302, 1280, 1259, 1208, 1169, 1156, 1130, 1120, 1072, 1036, 955, 832, 766, 752, 660, 637; ESMS calculated for $C_{40}H_{33}N_4O_4$ $[M+H]^+$ 633.2, found 633.2.

General Procedure Complex Synthesis [Ru(tpy)(L)(py)](PF$_6$)$_2$ complexes (L = 5–7). [Ru(tpy)Cl$_3$], Ardppn ligands (L) and LiCl were added to a pressure tube. Ethanol and water were added and the mixture was deoxygenated by bubbling Ar through a submerged needle for 20 min. Et$_3$N was added and the pressure tube was sealed and heated to 80 °C for 16 h. The reaction mixture was cooled to rt, concentrated and the residue was purified by column chromatography on neutral alumina to give [Ru(tpy)(L)(Cl)](Cl) as red solids. A solution of [Ru(tpy)(L)Cl]Cl in EtOH was treated with pyridine. Water was added and the mixture was deoxygenated by bubbling Ar through a submerged needle for 20 min. The pressure tube was sealed and heated to 80 °C for 16 h. The reaction mixture was cooled to rt, concentrated, and the residue was purified by column chromatography on alumina to give [Ru(tpy)(L)(py)](Cl)$_2$ complexes. Anion metathesis was accomplished by dissolving this compound in a minimal amount of H_2O and treating with a saturated aqueous solution of NH_4PF_6 to give the final compound that was isolated by filtration and dried *in vacuo* to give [Ru(tpy)(L)(py)](PF$_6$)$_2$ complexes.

[Ru(tpy)(Ph$_2$Me$_2$dppn)(py)](PF$_6$)$_2$ (8). Compound **8** was synthesized using the general procedure for complex synthesis starting from [Ru(tpy)Cl$_3$] (57 mg, 0.13 mmol), **5** (92 mg, 0.18 mmol) LiCl (28 mg, 0.65 mmol), EtOH (11 mL), water (5.5 mL) and Et$_3$N (0.22 mL, 1.6 mmol). The residue was purified by column chromatography on neutral alumina (2% MeOH:CH_2Cl_2) to give [Ru(tpy)(Ph$_2$Me$_2$dppn)(Cl)](Cl) as a red solid (83 mg, 70%). ^{1}H NMR (400 MHz, CD_3OD) δ 9.23 (d, *J* = 8.3 Hz, 1H), 8.60 (dd, *J* = 8.1, 4.0 Hz, 3H), 8.49 (d, *J* = 8.0 Hz, 2H), 8.11 (dd, *J* = 8.2, 4.6 Hz, 2H), 8.09 – 8.00 (m, 2H), 7.94 – 7.86 (m, 4H), 7.75 (qd, *J* = 7.5, 6.6, 3.6 Hz, 3H), 7.68 – 7.64 (m, 2H), 7.63 – 7.55 (m, 5H), 7.55 – 7.51 (m, 2H), 7.25 (ddd, *J* = 7.3, 5.6, 1.3 Hz, 2H), 7.16 (d, *J*

= 8.2 Hz, 1H), 3.47 (s, 3H), 1.70 (s, 3H). ESMS: calculated for $C_{51}H_{35}N_7Ru$ [M^{2+}] 423.5998, found 423.5557. The intermediate [Ru(tpy)(Ph_2Me_2dppn)Cl]Cl (41 mg, 0.045 mmol) was treated with EtOH (5 mL), pyridine (0.014mL, 0.18 mmol) and water (5 mL). The residue was purified by column chromatography on alumina (3-4%MeOH in DCM) to give [Ru(tpy)(Ph_2Me_2dppn)(py)]$(Cl)_2$ (30 mg, 67%). Anion metathesis gave [Ru(tpy)(Ph_2Me_2dppn)(py)]$(PF_6)_2$ (**8**, 30 mg, 83%) as a black solid. ^{1}H NMR (400 MHz, Acetonitrile-d_3) δ 9.25 (d, J = 8.3 Hz, 1H), 8.75 (d, J = 8.2 Hz, 1H), 8.52 (d, J = 8.2 Hz, 2H), 8.44 (dt, J = 7.9, 1.1 Hz, 2H), 8.24 – 8.12 (m, 4H), 8.07 – 8.02 (m, 3H), 7.99 – 7.96 (m, 2H), 7.85 – 7.77 (m, 5H), 7.74 – 7.64 (m, 8H), 7.61 – 7.59 (m, 2H), 7.41 – 7.36 (m, 2H), 7.26 (d, J = 8.2 Hz, 1H), 7.12 – 7.06 (m, 1H), 2.19 (s, 3H), 1.68 (s, 3H); IR (KBr) 2924, 2853, 2802, 2661, 2361, 2342, 1490, 1449, 1420, 1389, 1361, 1348, 1299, 1285, 1240, 1208, 1142, 1072, 1032, 953, 839, 768, 702, 670; UV-Vis: λ_{max} 489 nm (ε = 11,400 $M^{-1}cm^{-1}$); ESMS Calculated for $C_{56}H_{40}F_6N_8PRu$ [M^+] 1071.2, found 1071.2; Anal. Calcd. for $C_{56}H_{44}F_{12}N_8O_2P_2Ru$ (**8**·$2H_2O$): C, 53.72; H, 3.54; N, 8.95. Found: C, 53.96; H, 3.82; N, 8.82.

[Ru(tpy)(Me_2(2,4-Me_2Ph_2)dppn)(py)]$(PF_6)_2$ (**9**). Compound **9** was synthesized using the general procedure for complex synthesis starting from [Ru(tpy)Cl_3] (62 mg, 0.14 mmol), **6** (120mg, 0.2mmol) LiCl (30 mg, 0.7 mmol), EtOH (12 mL), water (6 mL) and Et_3N (0.24 mL, 1.7 mmol). The residue was purified by column chromatography on neutral alumina (2% MeOH:CH_2Cl_2) to give [Ru(tpy)(Me_2(2,4-Me_2Ph_2)dppn)(Cl)](Cl) as a red solid (83 mg, 70%). ^{1}H NMR (400 MHz, CD_3OD) δ 9.23 (d, J = 8.3 Hz, 1H), 8.68 – 8.57 (m, 3H), 8.50 (t, J = 8.6 Hz, 2H), 8.11 (t, J = 8.6 Hz, 2H), 8.02 – 7.81 (m, 6H), 7.56 (hept, J = 5.1 Hz, 2H), 7.46 (s, 1H), 7.38 – 7.17 (m, 8H), 3.47 (s, 3H), 2.61 (s, 3H), 2.49 (s, 3H), 2.02 (d, J = 2.0 Hz, 3H), 1.89 (d, J = 2.3 Hz, 3H), 1.73 (s, 3H); ESMS calculated for $C_{55}H_{43}ClN_7Ru$ [M^+] 938.2, found 938.2. The intermediate

[Ru(tpy)((Me$_2$(2,4-Me$_2$Ph$_2$)dppn)Cl]Cl was treated with EtOH (6 mL), pyridine (0.013 mL, 0.16 mmol) and water (6 mL). The residue was purified by column chromatography on alumina (3-4%MeOH in DCM) to give [Ru(tpy)(Me$_2$(2,4-Me$_2$Ph$_2$)dppn)(py)](Cl)$_2$ (30 mg, 71%).^{1}H NMR (400 MHz, Methanol-d_4) δ 9.33 (d, J = 8.3 Hz, 1H), 8.82 (d, J = 8.2 Hz, 1H), 8.72 (dt, J = 7.7, 4.6 Hz, 2H), 8.67 – 8.60 (m, 2H), 8.25 (t, J = 8.2 Hz, 1H), 8.18 – 8.05 (m, 5H), 7.92 – 7.84 (m, 2H), 7.80 – 7.72 (m, 3H), 7.63 – 7.57 (m, 2H), 7.51 – 7.42 (m, 3H), 7.37 – 7.32 (m, 4H), 7.26 (d, J = 1.9 Hz, 2H), 7.17 (t, J = 6.9 Hz, 2H), 2.61 (s, 3H), 2.50 (s, 3H), 2.25 (s, 3H), 2.03 (d, J = 1.7 Hz, 3H), 1.92 (d, J = 2.4 Hz, 3H), 1.74 (s, 3H). Anion metathesis gave [Ru(tpy)((Me$_2$(2,4-Me$_2$Ph$_2$)dppn)(py)](PF$_6$)$_2$ (**9**, 32 mg, 75%) as a black solid. ^{1}H NMR (400 MHz, CD$_3$CN) δ 9.20 (d, J = 8.3 Hz, 1H), 8.71 (d, J = 8.2 Hz, 1H), 8.56 – 8.38 (m, 6H), 8.19 (t, J = 8.2 Hz, 2H), 8.04 (dd, J = 16.0, 7.4 Hz, 4H), 7.97 – 7.89 (m, 3H), 7.72 (t, J = 7.6 Hz, 2H), 7.67 – 7.57 (m, 4H), 7.52 (s, 1H), 7.40 (s, 4H), 7.32 – 7.24 (m, 4H), 7.09 (q, J = 6.1 Hz, 2H), 2.64 (s, 3H), 2.53 (s, 3H), 2.18 (s, 3H), 2.11 (s, 3H), 2.06 (s, 3H), 1.68 (s, 3H); IR (KBr) 3073, 3032, 2922, 2854, 2361, 2342, 1671, 1604, 1507, 1490, 1422, 1388, 1349, 1302, 1285, 1236, 1143, 1061, 1015, 994, 957, 840, 767, 740, 699; UV-Vis: λ_{max} 487 nm (ε = 12,000 M^{-1}cm^{-1}); ESMS Calculated for $C_{60}H_{48}F_6N_8PRu$ [M$^+$] 1127.2, found 1127.2; Anal. Calcd. for $C_{60}H_{54}F_{12}N_8O_3P_2Ru$ (**9**·3H$_2$O): C, 54.34; H, 4.10; N, 8.45. Found: C, 54.29; H, 4.17; N, 8.38.

[Ru(tpy)(Me$_2$(2,4-(MeO)$_2$Ph$_2$)dppn)(py)](PF$_6$)$_2$ (10). Compound **10** was synthesized using the general procedure for complex synthesis starting from [Ru(tpy)Cl$_3$] (48mg, 0.11mmol), **7** (95 mg, 0.15 mmol) LiCl (23 mg, 0.55 mmol), EtOH (8 mL), water (4 mL) and Et$_3$N (0.18 mL, 1.3 mmol). The residue was purified by column chromatography on neutral alumina (2% MeOH:CH$_2$Cl$_2$) to give [Ru(tpy)((2,4-(MeO)$_2$Ph$_2$)dppn))(Cl)](Cl) as a red solid (41 mg, 36%). ^{1}H NMR (400 MHz, Methanol-d_4) δ 9.28 (dd, J = 8.3, 1.7 Hz, 1H), 8.70 – 8.57 (m, 3H), 8.52 – 8.46 (m, 2H), 8.10 (dt,

J = 8.1, 3.9 Hz, 2H), 7.99 – 7.85 (m, 6H), 7.55 – 7.47 (m, 2H), 7.42 – 7.32 (m, 1H), 7.30 – 7.15 (m, 4H), 6.96 (t, *J* = 2.7 Hz, 1H), 6.88 (dt, *J* = 8.3, 2.4 Hz, 1H), 6.81 (dd, *J* = 6.3, 2.4 Hz, 1H), 6.72 (ddd, *J* = 15.8, 8.3, 2.4 Hz, 1H), 4.05 (d, *J* = 2.3 Hz, 3H), 3.93 (d, *J* = 1.9 Hz, 3H), 3.69 (dd, *J* = 11.9, 2.4 Hz, 3H), 3.55 (dd, *J* = 14.6, 2.4 Hz, 3H), 3.46 (d, *J* = 1.5 Hz, 3H), 1.70 (d, *J* = 14.4 Hz, 3H); HRMS(ESMS) calculated for $C_{55}H_{43}ClN_7O_4Ru$ $[M]^+$ 1002.2, found 1002.2. The intermediate [Ru(tpy)((2,4-$(MeO)_2Ph_2$)dppn))Cl]Cl (35 mg, 0.034mmol) was treated with EtOH (5 mL), pyridine (0.010 mL, 0.14 mmol) and water (5 mL). The residue was purified by column chromatography on alumina (3-4%MeOH in DCM) to give [Ru(tpy)((2,4-$(MeO)_2Ph_2$)dppn))(py)]$(Cl)_2$ (30 mg, 79%).^{1}H NMR (400 MHz, Methanol-d_4) δ 9.40 (dd, *J* = 8.4, 1.6 Hz, 1H), 8.88 (d, *J* = 8.2 Hz, 1H), 8.72 (d, *J* = 8.2 Hz, 2H), 8.64 (d, *J* = 8.3 Hz, 2H), 8.29 – 8.22 (m, 1H), 8.11 (td, *J* = 9.4, 8.7, 5.5 Hz, 4H), 7.98 (dd, *J* = 13.2, 7.1 Hz, 2H), 7.80 – 7.72 (m, 3H), 7.60 – 7.52 (m, 2H), 7.51 – 7.43 (m, 3H), 7.45 – 7.26 (m, 4H), 7.23 – 7.14 (m, 2H), 7.01 – 6.89 (m, 2H), 6.87 – 6.77 (m, 2H), 4.06 (d, *J* = 1.7 Hz, 3H), 3.99 – 3.90 (m, 3H), 3.74 – 3.66 (m, 3H), 3.63 – 3.56 (m, 3H), 2.29 – 2.24 (m, 3H), 1.74 (d, *J* = 4.6 Hz, 3H). Anion metathesis gave [Ru(tpy)((2,4-$(MeO)_2Ph_2$)dppn)(py)]$(PF_6)_2$ (**10**, 27 mg, 82%) as a black solid. ^{1}H NMR (400 MHz, Acetonitrile-d_3) δ 9.29 (d, *J* = 8.3 Hz, 1H), 8.79 (d, *J* = 8.2 Hz, 1H), 8.53 (dd, *J* = 9.1, 4.4 Hz, 2H), 8.47 – 8.42 (m, 2H), 8.19 (t, *J* = 8.0 Hz, 2H), 8.03 (dd, *J* = 12.4, 7.5 Hz, 6H), 7.72 (t, *J* = 7.8 Hz, 2H), 7.62 (dd, *J* = 11.4, 5.9 Hz, 4H), 7.38 (p, *J* = 7.7, 7.0 Hz, 3H), 7.28 (d, *J* = 8.3 Hz, 1H), 7.10 (d, *J* = 6.9 Hz, 2H), 7.02 (t, *J* = 3.2 Hz, 1H), 6.96 (d, *J* = 8.6 Hz, 1H), 6.89 (s, 1H), 6.84 (d, *J* = 8.6 Hz, 1H), 4.08 (s, 3H), 3.98 (s, 3H), 3.74 (d, *J* = 11.9 Hz, 3H), 3.62 (d, *J* = 10.0 Hz, 3H), 2.18 (s, 3H), 1.69 (s, 3H); IR (KBr) 2928, 2841, 2360, 2342, 1607, 1578, 1509, 1497, 1449, 1418, 1389, 1349, 1302, 1283, 1262, 1209, 1156, 1108, 1081, 1032, 955, 840, 768, 741, 699, 669; UV-vis λ_{max} 487 nm (Ɛ = 10,600 $M^{-1}cm^{-1}$); ESMS Calculated for $C_{60}H_{48}F_6N_8O_4PRu$ $[M^+]$ 1191.2, found 1191.2;

Anal. Calcd. for $C_{60}H_{52}F_{12}N_8O_6P_2Ru$ (**10**·$2H_2O$): C, 52.52; H, 3.82; N, 8.17. Found: C, 52.39; H, 4.00; N, 8.21.

LogP. Solutions of **1** and **8**–**10** were prepared in octanol (2 mL, 100 μM) and combined with deionized water (2 mL) in glass vials. The vials were capped, wrapped in aluminum foil, shaken (5 min), and allowed to settle (24 h). After 24 h, relative concentrations of **1** and **8**–**10** in the water and octanol layers were determined spectrophotometrically using absorbance values at 490 nm. LogP was calculated using the quotient of the absorbance at 490 nm in octanol over the absorbance at 490 nm in water.

EC_{50} Determinations. MDA-MB-231 cells or DU-145 cells were seeded in a 96-well plate at the density of 7,000 cells per well in 100 μL of Dulbecco's modified Eagle's medium (DMEM) containing 10% FBS and 1,000 units/mL penicillin/streptomycin. Each plate was incubated in a 37 °C humidified incubator ventilated with 5% CO_2 overnight (16 h). The media was aspirated from each well and quadruplicate wells were treated with media containing **1, 8**–**10** (100 μM–100 nM) in 1% DMSO. Plates also contained blank wells with no cells and control wells with media containing 1% DMSO. After 1 h of incubation at 37 °C, plates were irradiated using a blue LED light source (see SI, t_{irr} = 15 min, λ_{irr} = 460–470 nm, 170 J/cm^2) or left in the dark and incubated for either 4 or 72 h in a 37 °C humidified incubator ventilated with 5% CO_2. After incubation, MTT reagent (10 μL, 5 mg/mL in PBS) was added to each well and plates were kept at 37 °C and 5% CO_2 for 2 h. The media was aspirated from each well and DMSO (100 μL) was added. The wells were shaken for 30 min to allow for the solvation of the formazan crystals. Absorbance at 570 nm was measured in each well. Average absorbance values for the blank wells were subtracted from absorbance values for each sample to eliminate background. Viability data were obtained by

averaging normalized absorbance values for untreated cells and expressing absorbance for the treated samples as percent control. EC_{50} values were determined using Igor Pro graphing software.

Flow Cytometry Analysis. MDA-MB-231 cells were seeded at 250,000 cells/plate in five 60 mm^2 cell culture dishes containing 3 mL of DMEM treated with 10% FBS and 1,000 units/mL penicillin/streptomycin. After seeding, the cells were incubated at 37 °C and 5% CO_2 overnight (18 h). After incubation, two plates were treated with compound **1** (10 μM) or **9** (20 μM) in media (1% DMSO) and set to incubate at 37 °C and 5% CO_2 for 1 h. The remaining two plates were treated with DMEM containing 1% DMSO and placed in the incubator. Following incubation, plates were irradiated using a blue LED light source (see SI, t_{irr} = 15 min, λ_{irr} = 460–470 nm, 170 J/cm^2) or left in the dark. These plates were incubated at 37 °C and 5% CO_2 for 4 h. After 4 h incubation, both the irradiated and non-irradiated plates were removed from the incubator. In a separate plate, after 2 h, cells treated with vehicle alone had media removed and replaced with H_2O_2 (500 mM) in PBS. Cells were incubated at 37 °C and 5% CO_2 for 3 h. The media from each plate was saved in a 15 mL falcon tube. The cells were detached from each plate via trypsinization and added to the previously removed media. The cells were centrifuged (600 g, 5 min) to pellet the cells. The supernatant was decanted, and the pellet was washed twice with PBS (4 mL). After the final wash, the supernatant was decanted, and the pellet was suspended in PBS (100 μL). A solution of Annexin V (5 μL, 1 mg/mL) was added to the cell suspension. The suspension was incubated at rt (15 min). After incubation, PBS was added (1 mL) to the tube and the suspension was centrifuged (600 g, 5 min). The supernatant was decanted and cells were suspended in PBS (100 μL). A solution of propidium iodide (5 μL, 12 μM) was added to the cell suspension and incubated at rt (15 min). The cell suspension was diluted with PBS (1 mL). The suspension was passed through a metal mesh filter (30 μm) from Celltrics (Kobe, Hyōgo Prefecture, Japan) into a

small sample tube. Flow cytometric analysis was performed on a Sysmex Cyflow Space fluorescence assisted cell sorter. Data was processed using FCS Express.fcs processing software by De Novo software (Boulder, Co)**.**

ROS Scavenging. MDA-MB-231 cells were seeded in a 96-well plate at the density of 7,000 cells per well in DMEM (100 μL) containing 10% FBS and 1,000 units/mL penicillin/streptomycin and incubated at 37 °C and 5% CO_2 overnight. Each plate contained blank wells containing no cells and control wells with cells containing media and 1% DMSO. Non-control or non-blank wells were treated with compound **1** (10 μM) or **9** (20 μM) in media (1% DMSO) containing either NaN_3 (50 mM), mannitol (50 mM), histidine (50 mM), or N-acetyl cysteine (5 mM) in quadruplicate. Plates were incubated at 37 °C and 5% CO_2 for 1 h and irradiated using a blue LED light source (see SI, t_{irr} = 15 min, λ_{irr} = 460–470 nm, 170 J/cm^2) for 15 min. After 4 h incubation, MTT assay was used to assess viability as described above.

Results and Discussion

Synthesis and Structural Characterization

A literature search revealed that derivatives of dppn were limited to brominated (Br_2dppn), quinone (qdppn) and trialkylsilylalkyne derivatives ((i-$Pr_3SiCC)_2$dppn) (Figure 2). Prior investigations with trialkylsilylalkyne derivatives used Sonogashira cross coupling reactions with 4,9-dibromonaphtho[2,3-*c*][1,2,5]thiadiazole to install alkyne substituents.[62] Subsequent reduction with $LiAlH_4$, followed by condensation of the resultant diamine with 1,10-phenanthroline-5,6-dione gave trialkylsilylalkyne dppn derivatives functionalized in the 10- and 15-positions. Although this synthetic sequence provided the ligands in good overall yields, this strategy required a multi-step synthesis to access each new dppn derivative. Instead of using early-stage cross

coupling reactions with 4,9-dibromonaphtho[2,3-*c*][1,2,5]thiadiazole, we envisioned a divergent approach, where new aryl substituents could be introduced at the latest stage, after formation of the dppn ring system. This new strategy required the synthesis of Br_2Me_2dppn (**4**). Compound **4** was accessed by condensation of 2,9-dimethyl-1,10-phenanthroline-5,6-dione (**2**)[63] with 1,4-dibromonaphthalene-2,3-diamine (**3**),[43] which is available in one step via bromination of 2,3-diaminonapthalene.[61] Suzuki cross coupling of **4** with three aryl boronic acids provided the diphenyl (**5**), di(2,4-dimethylphenyl) (**6**) and di(2,4-dimethoxyphenyl) (**7**) substituted ligands in one step from **4** in good yields (55–57%). Ligands **5**–**7** were chosen to probe steric and electronic effects in their respective Ru(II) complexes. Diphenyl derivative **5** was designed to act as a standard. Introducing the 2-methyl group, as shown with **6**, was expected to minimize overlap of the dppn and phenyl π-systems due to allylic strain (Figure 3). In addition, the 2- and 4-methyl groups on the phenyl groups of **6** were expected to provide a mild electron-donating effect, and also increase lipophilicity and solubility of resultant Ru(II) complexes. The 2,4-dimethoxy substituents on ligand **7** were expected to provide stronger electron donation than the methyl groups of **6,** but were also expected to minimize overlap of the dppn and phenyl π-systems due to allylic strain and increase solubility. Attempts were also made to couple 2,4,6-trimethylphenyl boronic acid with **4** using the same coupling conditions and other protocols for sterically-demanding Suzuki reactions. However, complex mixtures were obtained, with no evidence of dual coupling by ^{1}H NMR spectroscopy or ESMS. The inability to obtain product from 2,4,6-trimethylphenyl boronic acid is likely due to the steric environment of the bromides in **4**, with ortho C-H and N functional groups, which is highly crowded.

Figure 3. Space-filling models of the ligands A) Me_2dppn (**1**) and B) $Me_2(Ph)_2$dppn (**5**)

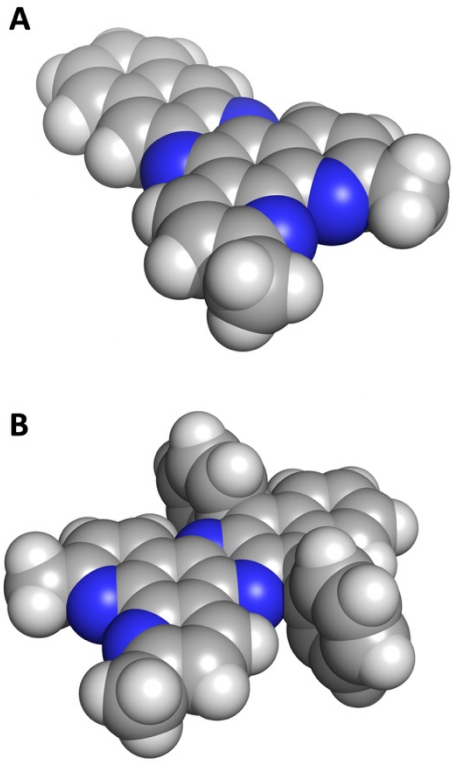

Scheme 1. Synthesis of aryl-substituted dppn derivatives **5**–**7**

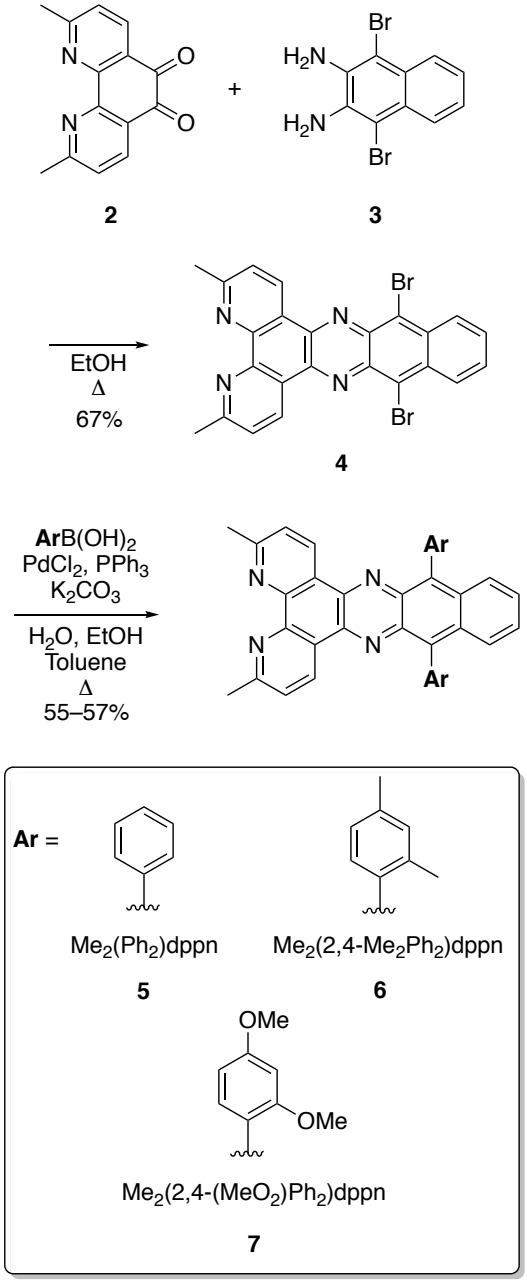

Three Ru(II) complexes derived from the arylated ligands **5**–**7** were prepared using a two-step synthetic procedure starting from [Ru(tpy)Cl_3] (Scheme 2). Treating **5**–**7** with [Ru(tpy)$(Cl)_3$], LiCl and Et_3N in a mixture of EtOH and H_2O at 80 °C provided access to chloride complexes with the general formula [Ru(tpy)(L)(Cl)]Cl, where L = **5**–**7**. Subsequent treatment of these salts with excess pyridine (4.0 equiv) in 1:1 EtOH:H_2O, followed by salt metathesis with NH_4PF_6 provided the final complexes **8**–**10** containing monodentate pyridines with the general formula [Ru(tpy)(L)(py)]$(PF_6)_2$, where L = **5**–**7** in 28–53% yield over two steps.

Ru(II) complexes were characterized by ^{1}H NMR, IR, and electronic absorption spectroscopies, electrospray mass spectrometry, and elemental analysis. A key feature noted in the ^{1}H NMR spectra of **8**–**10** is the loss of symmetry that occurs upon binding of ligands **5**–**7** to the Ru(II) center. For instance, the ^{1}H NMR spectrum of ligand **5** shows one resonance in the aliphatic region assigned to the 3- and 6-methyl groups; in contrast, the ^{1}H NMR spectrum of complex **8** shows two resonances for methyl groups, similar to **1**, which arise from the different chemical environments of the two methyl groups upon coordination to the $[Ru(tpy)(py)]^{2+}$ fragment. Spectra for ligands **6** and **7** show three singlets in the aliphatic region (~4.1–1.9 ppm) integrating for 6 protons each, which are assigned to NMR equivalent methyl groups that are related by a C_2 axis and mirror plane that bisects the nitrogen atoms of **5**–**7**. Complexes **9** and **10** each show 6 resonances integrating for three protons each from 4.2–1.5 ppm, which are assigned to the six methyl groups in the complexes that each are in different chemical environments. Interestingly, resonances for methoxy groups of **10** at ~3.6 and ~3.4 ppm appear as overlapping broad singlets that collectively integrate for three protons each. The splitting of these resonances into two peaks is consistent with the presence of *cis* and *trans* atrope isomers, which would be expected to undergo slow interconversion on the NMR timescale, due to the crowded steric environment of the Ar-

C(Me$_2$dppn) bond (Figure S2). ESMS spectra of complexes **8**–**10** show major molecular ions with suitable isotopic distributions at 1071.2, 1127.2, and 1191.2, which are consistent with cations [[Ru(tpy)(**5**)(py)](PF$_6$)]$^+$, [[Ru(tpy)(**6**)(py)](PF$_6$)]$^+$, and [[Ru(tpy)(**7**)(py)](PF$_6$)]$^+$, respectively.

Scheme 2. Synthesis of ruthenium complexes of the general formula [Ru(tpy)(L)(Py)](PF$_6$)$_2$ (**8**–**10**), where L = aryl-substitued dppn derivatives **5**–**7**.

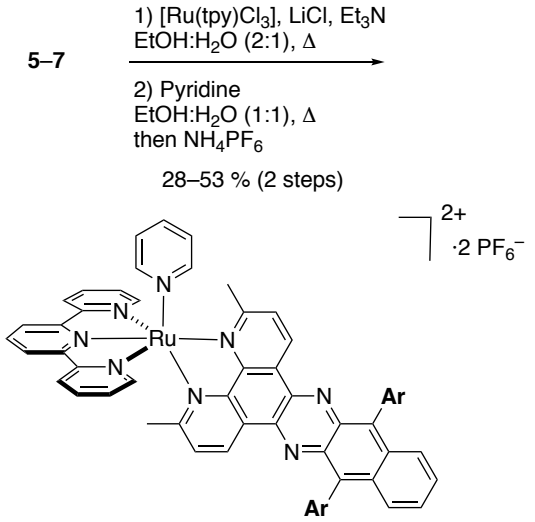

[Ru(tpy)(Me$_2$(Ph$_2$)dppn)(py)](PF$_6$)$_2$ (**8**)

[Ru(tpy)(Me$_2$(2,4-Me$_2$Ph$_2$)dppn)(py)](PF$_6$)$_2$ (**9**)

[Ru(tpy)(Me$_2$(2,4-(MeO$_2$)Ph$_2$)dppn)(py)](PF$_6$)$_2$ (**10**)

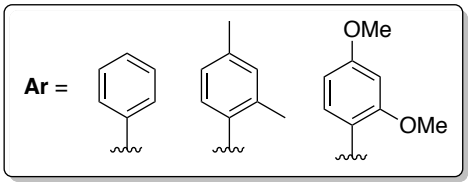

Photophysical Properties and Photochemistry

Complexes **8**–**10** in MeOH exhibit strong electronic absorption in the visible region, with peaks that tail out to ~700 nm, as depicted in Figure 4. Importantly, the spectral profiles of complexes **8**–**10** are similar to those of **1** (Figure 4). Ligand-centered $^1\pi\pi^*$ transitions associated with the py and tpy ligands are observed in the 200–350 nm range, as previously reported for the related complexes $[Ru(tpy)(bpy)(py)]^{2+}$ and $[Ru(tpy)(dppn)(py)]^{2+}$.[14,15] In addition, dppn-centered $^1\pi\pi^*$ absorption features at ~400 are also observed for **1** and **8**–**10**, consistent with the similarity of the electronic structure of this ligand.[14,15,27] In addition, the maxima of the broad Ru(dπ)→tpy(π*) metal-to-ligand charge transfer (MLCT) bands of **8**–**10** appear at ~480–490 nm, at a similar position to that of **1** and related Ru(II)-dppn complexes.[14,15,27,30]

It should also be noted that a red shift in the ^{1}MLCT absorption is not observed across the series, indicating that the attachment of the aryl groups does not significantly shift the absorption to longer wavelengths, as expected from related complexes with substitutions to the distal portion of the dppz and dppn ligands.[64-69] It has been established that in this type of complexes the ^{1}MLCT transition observed with high intensity takes place from the Ru-centered HOMO to a molecular orbital on the dppz or dppn ligand with electron density proximal to the metal owing to greater spatial overlap.[64-69] Although a lower energy MLCT state from the Ru to the distal fragment of the ligand is present, its optical density is negligible, such that substitutions to this part of the dppn or dppz ligand do not result in marked changes in energy or intensity to the absorption in the visible range.[64-69]

Figure 4. Electronic absorption spectra of **1** (black), **8** (green), **9** (red) and **10** (blue) in MeOH.

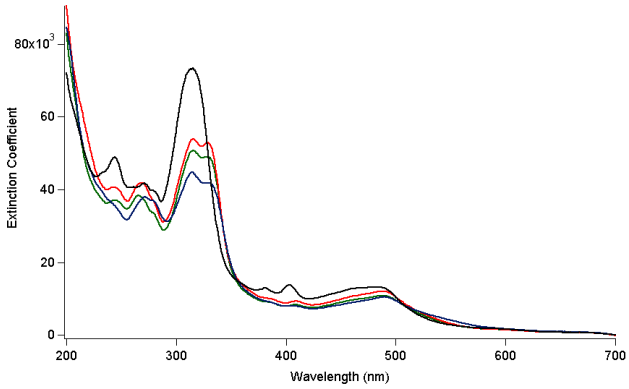

Irradiation of **8** – **10** in MeCN with λ_{irr} = 500 nm results in the exchange of the monodentate pyridine ligand for the coordinating solvent, whereas no exchange is observed under similar experimental conditions in the dark over a period of at least 22 hrs. The ligand exchange processes for **8**, **9**, and **10** in MeCN occur with quantum yields (Φ_{500}) of 0.13(4), 0.13(3), and 0.13(2), respectively, more efficiently than non-arylated Me_2dppn derivatives **1** and $[Ru(tpy)(Me_2dppn)(imatinib)]^{2+}$ (Table 1). The reason for the greater ligand exchange quantum yields of **8**–**10** is not readily apparent and is still under investigation. In addition to photoinduced ligand exchange, **8**, **9**, and **10** produce $^1O_2$ following visible light irradiation with quantum yields, Φ_Δ, of 0.62(3), 0.61(3), and 0.56(4), respectively, all of which are slightly lower than that of **1** (**Table 1**). The reduced efficiency of $^1O_2$ production may be attributed to competitive population of the competing ^{3}MC (metal-centered) state(s) in **8**–**10** as compared to **1**, as evidenced by higher ligand exchange quantum yields.

The excited state dynamics of **8** – **10** were investigated using nanosecond transient absorption (TA) spectroscopy in pyridine to preclude the formation of a new product stemming from ligand photosubstitution with the solvent. The TA spectrum of **8** in deaerated pyridine, shown in Figure 5, features strong positive signals centered at ~365 and 580 nm that decay

monoexponentially with τ = 47 μs (λ_{exc}=500 nm, fwhm = 8 ns). TA spectra with similar features were collected for **9** and **10** with lifetimes of 50 and 46 μs, respectively (Figures S6–S7). The strong signal at ~580 nm is known to be associated with the population of the dppn-localized $^3\pi\pi^*$ excited state, in this case on the arylated Me_2dppn ligand, and is consistent with TA spectra and lifetimes reported for other Ru(II) complexes containing the dppn ligand such as **1** (τ = 47 μs), $[Ru(tpy)(dppn)(py)]^{2+}$ (τ = 50 μs), and $[Ru(bpy)_2(dppn)]^{2+}$ (τ = 33 μs).[15,66,70] The existence of a long-lived excited state is necessary for the efficient bimolecular energy transfer to ground state $^3O_2$ to produce cytotoxic $^1O_2$. Similar excited state lifetimes in **1** and **8**–**10** demonstrate that the aryl substitutions on the Me_2dppn ligand do not significantly affect the electronic or photophysical properties of the complex.

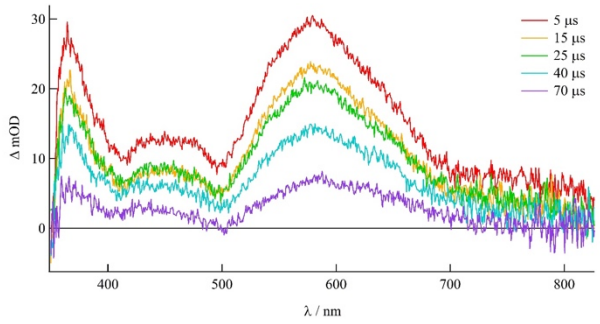

Figure 5. Transient absorption spectrum of **8** in deaerated pyridine (λ_{exc} = 500 nm, 5.9 mJ/pulse, fwhm = 8 ns).

Table 1. Quantum yields for ligand exchange (Φ_{500}) and $^1O_2$ production singlet oxygen (Φ_Δ) for **1**, **8**–**10**, and related Ru(II) complexes, and their octanol-water partition coefficients (LogP).

Compound	Φ_{500}[a]	Φ_Δ[b]	Log P[c]
1	0.053(1)[15]	0.69(9)[15]	–0.27 ± 0.06
8	0.13(4)	0.62(3)	0.11 ± 0.01
9	0.13(3)	0.61(3)	0.32 ± 0.03
10	0.13(2)	0.56(4)	0.23 ± 0.03
[Ru(tpy)(Me$_2$dppn)(imatinib)]$^{2+}$	0.073(1)[72]	0.57(7)[72]	ND[d]

[a]MeCN, λ_{irr} = 500 nm. [b]MeOH, λ_{irr} = 460 nm, 435 longpass filter. [c]Shake flask method, 298 ± 3 K, results are average of three independent experiments, errors are standard deviations. [d]Not determined.

DNA Binding

A number of techniques are typically required to understand the mode of binding between metal complexes and DNA, including spectrophotometric titrations, relative viscosity measurements, and thermal denaturation. Upon intercalation to DNA, the electronic absorption spectrum of a complex containing a ligand with an extended π-system exhibits hypochromism and modest bathochromism due to π-stacking interactions between the complex and the DNA bases.[71,72] The titration of DNA up to 100 μM bases to 5 μM solutions of **8**–**10** resulted in hypochromic shifts of the MLCT transition of 16% in **8**, 38% in **9**, and 36% in **10** and no discernable bathochromic shifts. (Figure 6, S3–5).

It should be noted that changes in absorption upon the addition of DNA are known to be associated with π-stacking interactions, such as intercalation, but similar spectral shifts are also observed upon self-aggregation, enhanced aggregation in the presence of the polyanion, and other

hydrophobic interactions in the major and minor groove of DNA. The addition of polystyrene sulfonate (PSS) to cationic complexes has been previously used to probe the role of random coil polyanion on aggregation without the possibility of intercalation.[58] The electronic absorption spectra of 5 μM solutions of **8**–**10**, upon addition of 100 μM PSS, exhibit hypochromicity but to a lesser extent than 100 μM DNA bases (Figures S3–5). These results demonstrate that there is some π-stacking interaction in the presence of both polyanions, likely enhanced by electrostatic interactions between the cationic Ru(II) complexes and the anionic backbones of PSS and DNA, such that they cannot be assigned to intercalation between DNA base pairs.[58] Similar changes in absorption following addition of PSS are observed as a result of self-aggregation, as well as aggregation induced by the polyanion, as previously shown for cationic dirhodium complexes with dppz ligands.[58] Given the number of equilibria possible in solution with similar spectral changes, a binding constant cannot be determined from absorption titration measurement, as is typically calculated for these type of complexes and other intercalators.[73-75]

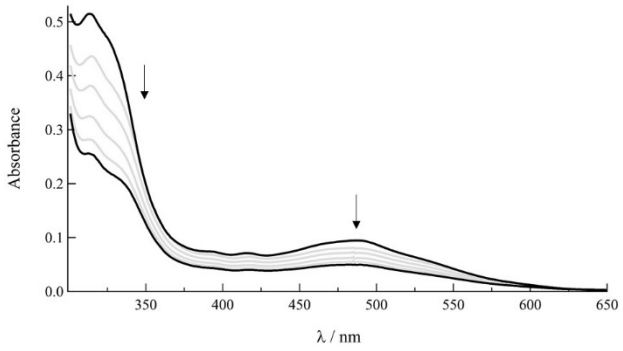

Figure 6. Changes in the electronic absorption spectrum of **8** (10 μM) after addition of 0, 20, 40, 60, 100, and 200 μM DNA bases to solution (5 mM Tris, 50 mM NaCl, pH 7.0).

Two other important methods for the characterization of intercalation of organic molecules and inorganic complexes are the measurement of the changes in the DNA melting temperature

(thermal denaturation) and the relative viscosity of DNA solutions in the presence of the probe. Attempts to obtain DNA melting temperatures in the presence of **8**–**10** were unsuccessful due to the decomposition of the complexes at temperatures above 60 °C. Electrostatic interactions between cationic metal complexes and the anionic phosphate backbone of DNA do not affect the viscosity of a DNA solution. In contrast, the intercalation of a molecule between the π-stacked bases of a duplex is known to unwind and elongate the cylindrical double helix DNA structure, thus increasing the viscosity relative to DNA alone.[72,76] Figure 7 shows the changes of the relative viscosity of DNA solutions as a function of the concentration of ethidium bromide (EtBr), a known DNA intercalator, and complexes **8**–**10**. Figure 7 also displays data for $[Ru(bpy)_3]^{2+}$, a complex that exhibits weak electrostatic interactions with the phosphodiester backbone and is known to not intercalate between DNA bases.[77] As expected, EtBr increases the viscosity of the DNA solution as the amount of probe in solution is increased, while $[Ru(bpy)_3]^{2+}$ has no detectible effect on DNA solution viscosity. Complexes **8**–**10** follow the same trend as $[Ru(bpy)_3]^{2+}$ as the concentration of complex in solution increases, having little to no effect on the viscosity of DNA solutions. These results are consistent with an electrostatic and/or hydrophobic interaction between **8**–**10** and DNA, including complex self-aggregation aided by the anionic backbone, but not intercalation between the DNA bases.

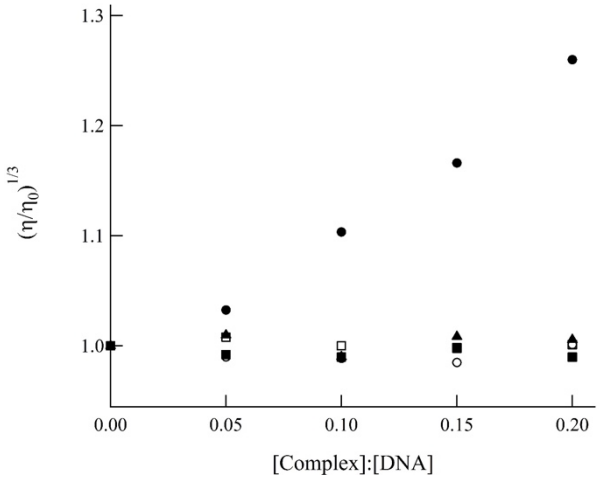

Figure 7. Relative viscosity of DNA (200 μM bases) solutions as a function of increasing concentration of $[Ru(bpy)_3]^{2+}$ (■), **8** (□), **9** (▲), **10** (○), and ethidium bromide (●).

Biological Characterization

Lipophilicity of compounds is often strongly correlated with the amount of cellular uptake. In general, the more lipophilic a compound is, the more able it is to penetrate the lipid bilayer of the outer plasma membrane. Although several passive and active forms of cellular uptake have been characterized for bioactive Ru(II) complexes,[6] many studies have established a positive correlation between lipophilicity, cell uptake, and cytotoxicity.[1] It is generally believed that increasing the lipophilicity of Ru(II) and related transition metal complexes through the addition of hydrophobic groups will lead to higher potency for cell killing.[1] In order to quantify lipophilicity, the partition coefficients (LogP) between water and octanol were determined for the parent Ru(II) complex **1**, which contains Me_2dppn, and the arylated derivatives **8**–**10** (Table 1). As predicted, the addition of aryl substituents onto the Me_2dppn ligand significantly enhanced lipophilicity in Ru(II) complexes **8**–**10** vs. complex **1**. Complex **1** shows a small, but negative Log P value, indicating that it prefers to dissolve in water vs. octanol by ~2:1 ratio. In contrast,

complexes **8**–**10** all show positive LogP values and prefer dissolution in octanol. The most lipophilic compound in the series was **9**, which contains the 2,4-dimethylphenyl groups, and is more lipophilic than **1** by over one order of magnitude. Complexes **10** and **8** showed lower LogP values than **9**, which is consistent with the nature of their substituents; phenyl would be expected to be less hydrophobic than 2,4-dimethoxyphenyl, which is in turn more polar than 2,4-dimethylphenyl due to the added oxygen atoms.

Given the photochemical reactivity and lipophilicity of Ru(II) complexes **8**–**10**, these compounds were evaluated alongside the parent Ru(II) complex **1** for growth inhibitory effects against MDA-MB-231 triple-negative breast cancer and DU-145 prostate cells, which are two aggressive cancer cell lines with high metastatic potential. Cells were treated with **1** or **8**–**10**, incubated for 1 h, then irradiated with a blue LED light source designed for 96 well plates (t_{irr} = 15 min, λ_{irr} = 460–470 nm, 170 J/cm^2). In parallel experiments, cells were treated in the same manner but were left in the dark. Effective concentrations to provide 50% growth inhibition (EC_{50}) values were determined 72 h after irradiation was concluded using the 3-(4,5-dimethylthiazol-2-yl)-2,5-diphenyltetrazolium bromide (MTT) assay (Table 2, entries 1–4). Phototoxicity indexes (PIs), which are the ratio of dark EC_{50} to light EC_{50}, were calculated for each complex and several trends were apparent in the data. First, complexes **8**–**10** all caused less potent growth inhibition against both MDA-MB-231 and DU-145 cell lines than **1** by a factor of 2–3. The Me_2dppn derivative **1** was the most potent analog in both cell lines and showed a superior PI value in the MDA-MB-231 cell line relative to **8**–**10**. Second, Ru(II) complexes **1** and **8**–**10** all showed lower EC_{50} values in the DU-145 prostate cancer cell line relative to MDA-MB-231 by a factor of roughly two. Third, PI values for **1**, **8** and **10** were similar, > 5, in the DU-145 cell line. Given the fact that **8**–**10** are unable to intercalate in DNA, but **1** is, it is clear that DNA intercalation is not a

requirement for cancer cell toxicity or photoinduced cell death. Furthermore, EC_{50} values for **1** and **8**–**10** showed no correlation with LogP values (Table 1), indicating that increasing lipophilicity of these Ru(II) complexes does not lead to greater efficacy.

During experiments with **1** and **8**–**10**, clear changes in cancer cell morphology from dendritic to rounded, granular and detached were observed in cells treated with all compounds and light at time points as early as 4 h, well before the 72 h endpoint of the MTT assay. To probe for toxic effects on shorter timescales, EC_{50} determinations were repeated for **1** and **9**, which were the most potent of the tested compounds, 4 h after irradiation was concluded (Table 2, entries 5 and 6). These data confirmed that **1** and **9** were able to produce an almost immediate toxic effect in both the MDA-MB-231 and DU-145 cell lines. PI values were much higher for **1** at 4 h than at 72 h in both cancer cell lines, with the highest value, PI >56, in DU-145 cells. This large increase in PI values was due to the minimal amount of toxicity observed, as judged by MTT, at the highest concentrations tested. In both MDA-MB-231 and DU-145 cells, EC_{50} values for **1** at the 4 h time point were >100 μM. In contrast, complex **9** showed toxicity at 4 h in both cell lines in the dark. The EC_{50} value for **9** in the dark in DU-145 cells was roughly double that observed at 72 h, which raised the PI from 2.8 at 72 h to 5.3 at 4 h.

Table 2. EC_{50} values (μM) for **1**, **8**–**10** against MDA-MB-231 and DU-145 cells at time, t_{MTT}, 72[a] and 4 h[b]

			EC_{50} / μM					
			MDA-MB-231			DU-145		
Entry	Compound	t_{MTT} / h	Light	Dark	PI[c]	Light	Dark	PI[c]
1	**1**[a]	72	4.6 ± 0.5	34 ± 3	7.4	2.0 ± 0.2	11 ± 6	5.5
2	**8**[a]	72	13 ± 1	37 ± 5	2.8	6.5 ± 2.5	33 ± 6	5.1
3	**9**[a]	72	8.6 ± 0.5	21 ± 2	2.4	6.0 ± 1.0	17 ± 1	2.8
4	**10**[a]	72	16 ± 3	63 ± 10	3.9	5.3 ± 1.0	29 ± 8	5.5
5	**1**[b]	4	6.0 ± 3.2	>100	>17	1.8 ± 0.2	>100	>56
6	**9**[b]	4	18 ± 6	41 ± 11	2.3	7.2 ± 2.6	38 ± 13	5.3

[a,b]Cells treated with compound **1**, **8**–**10** for 1 h, then irradiated (t_{irr} = 15 min, λ_{irr} = 460–470 nm, 170 J/cm^2) or left in the dark, cell viabilities were determined by MTT 4 and 72 h after irradiation was complete. Data are average of three independent experiments using quadruplicate wells, errors are standard deviations. [c]PI = phototherapeutic index = ratio dark EC_{50}/light EC_{50}.

Although many Ru(II) complexes have shown promising activity in cancer cell lines, few investigations have probed the timescale or mechanism by which these complexes cause cell death.[78-92] With the exception of two complexes derived from non-steroidal anti-inflammatory drugs that showed an approximately equal amount of apoptosis and necrosis,[84] most Ru(II) complexes induce apoptosis as the dominant mechanism of cell death. Data with **1** and **9** show that early, photoactivated cell death is achieved in both triple-negative breast and prostate cancer cell lines. Except for dark toxicity observed with **1** at 72 h, data in Table 2 indicate that most of the cytotoxic effect of **1** and **9** are realized after only 4 h. Because of its programmed nature, death by

apoptosis usually occurs on a longer timescale and requires at least 24 h before major metabolic changes occur that are evident by assays such as MTT. On the other hand, necrosis can occur almost immediately after compound treatment.[93] To probe the mechanism of cell death, complexes **1** and **9** were evaluated against the MDA-MB-231 and DU-145 cell lines by flow cytometric analysis (Figure 8). Cells were treated with vehicle (1% DMSO), **1** (10 μM) or **9** (20 μM) for 1 h, then were treated with light (t_{irr} = 15 min, λ_{irr} = 460–470 nm, 170 J/cm^2) or left in the dark (Figure 4). In parallel experiments, MDA-MB-231 and DU-145 cells were treated with 500 mM H_2O_2, which causes rapid necrosis and serves as a positive control (Figure 8B, 8H). Cells were stained 4 h after conclusion of the irradiation with Annexin V, an antibody that recognizes the translocation of phosphatidylserine from the inner to the outer leaflet of the cell plasma membrane that is strongly associated with apoptosis, and propidium iodide, a cell-impermeable dye that is only able to enter cells after integrity of the plasma membrane is compromised. Because necrosis is accompanied by permeabilization of the outer plasma membrane, substantial uptake of propidium iodide is strongly associated with necrosis. Cells that show positive Annexin V staining and are negative for propidium iodide are considered apoptotic, whereas cells that stain for both dyes are considered necrotic because rupture of the plasma membrane allows entry of propidium iodide and Annexin V into cells. Data for **1** and **9** in both MDA-MB-231 and DU-145 cells indicate that necrosis is the primary mode of cell death at 4 h. In all cases, cells treated with **1** or **9** that are Annexin V positive and propidium iodide negative (apoptotic, lower right-hand quadrant) account for a minimal amount (<7%) of the total cell population. Cells treated with **1** or **9** in the light show substantial populations of cells that are Annexin V and propidium iodide positive, as high as 61% with treatment of MDA-MB-231 cells with **1** (10 μM) and light (Figure 8C). In both cell lines, treatment with light results in a substantial increase (~30%) of Annexin V and propidium iodide

positive cells that is consistent with necrosis. Higher populations of cells showing little to no propidium iodide uptake or Annexin V uptake (normal, lower left-hand quadrant) were observed in cells treated with **1** or **9** in the dark. Given that **1** is not toxic in MDA-MB-231 cells at a concentration of 10 μM in the dark as judged by MTT (Table 3, entry 5), yet some amount of Annexin V and propidium iodide staining is observed (Figure 4C), staining may be facilitated by fusion of dye-containing aggregates of **1** with the MDA-MB-231 cells.[94] Indeed, Ru(II) complexes derived from dppn and related ligands are known to aggregate in solution.[95,96] Analysis of **1** and **8**–**10** in PBS buffer by dynamic light scattering indicated that particles ranging in size from 100–300 nm are present in solution (Figure S22). Taken together, these data confirm that treatment of MDA-MB-231 and DU-145 cells with **1** or **9** and light leads to substantial populations of necrotic cells, with minimal apoptosis.

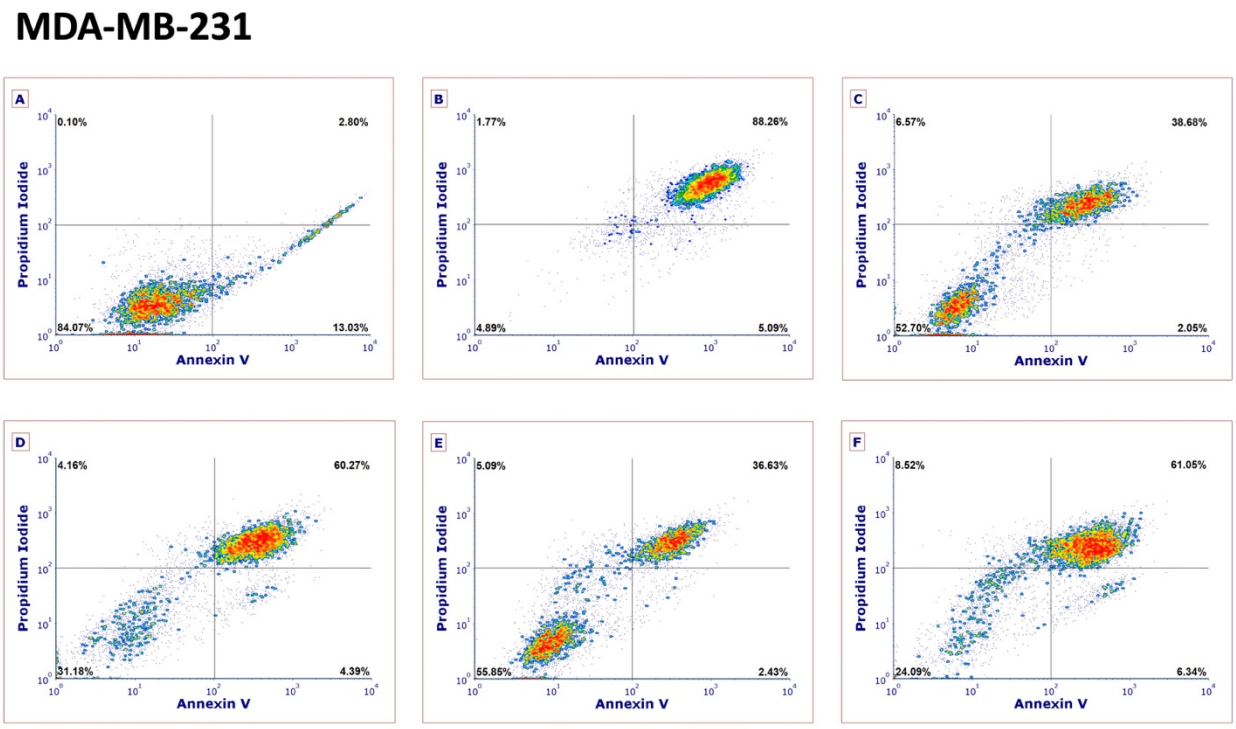

DU-145

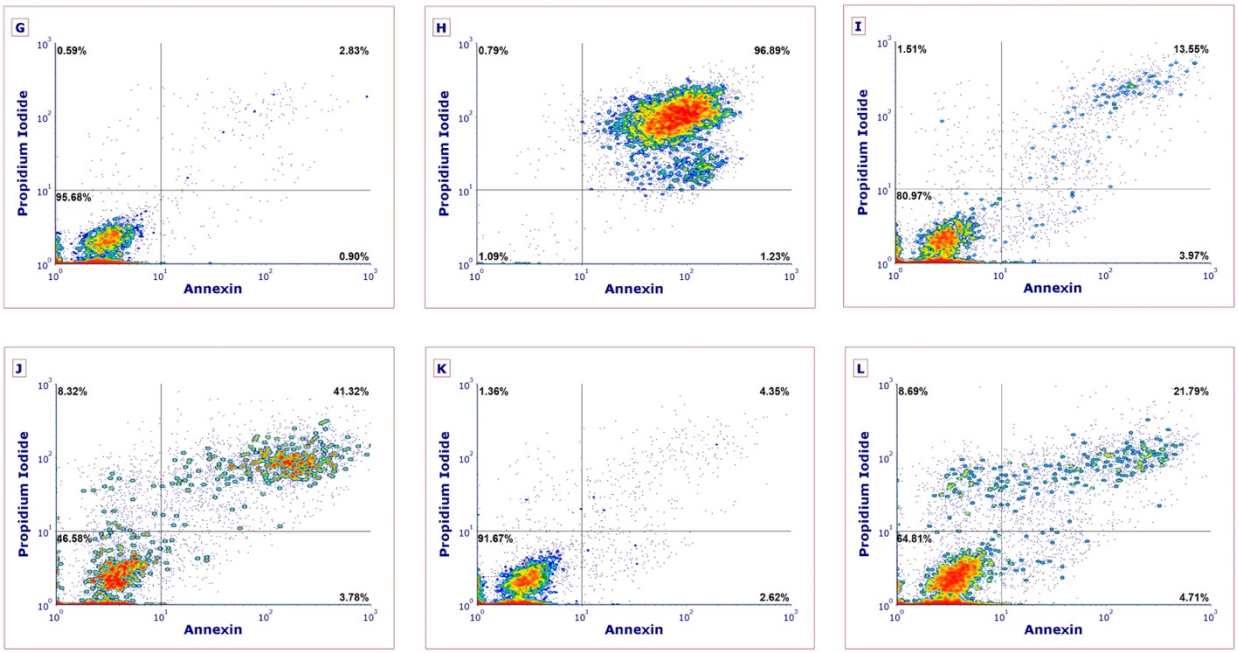

Figure 8. Flow cytometric analysis of MDA-MB-231 (A–F) and DU-145 (G–L) cells after 4 h treatment with **1** or **9** under dark and light (t_{irr} = 15 min, λ_{irr} = 460–470 nm, 170 J/cm^2) conditions using Annexin V/propidium iodide staining. Treatment conditions: A) vehicle and light; B) H_2O_2 (500 mM), 3 h treatment; C) **1** (10 μM) dark; D) **1** (10 μM) light; E) **9** (20 μM) dark; F) **9** (20 μM) light; G) vehicle and light; H) H_2O_2 (500 mM), 3 h treatment; I) **1** (10 μM) dark; J) **1** (10 μM) light; K) **9** (20 μM) dark; L) **9** (20 μM) light. Data are indicative of three independent experiments. See Supporting information for more details.

Data in this manuscript show that Ru(II) complexes **1** and **8**–**10** are dual action agents that show efficient photodissociation (PCT) and photosensitization (PDT) from the same molecular entity. Photochemical generation of reactive oxygen species (ROS) is the principle mode of action for PDT agents. With most investigations that describe new Ru(II)-based PDT agents, it is often assumed that cell-free assays that are used to detect the photochemical generation of ROS translate to ROS-induced death in cells. Although there are some exceptions,[39] researchers rarely use cell-

based assays to probe the role that ROS have in photoactivated death. The timescale of viability loss and flow cytometric data are both consistent with **1** and **9** causing necrotic cell death. In order to gain further insight into the mechanism of necrotic cell death, several ROS quenchers were examined for their ability to block cytotoxicity in MDA-MB-231 cells at 4 h. Cells were pretreated with sodium azide (50 mM), a quencher of singlet oxygen, histidine (50 mM) a quencher of hydroxyl radical that also scavenges singlet oxygen to a lesser extent than sodium azide,[97] and D-mannitol (50 mM), a hydroxyl radical scavenger. In addition, cells were pretreated with the antioxidant N-acetylcysteine (NAC, 5 mM),[98] which counteracts oxidative stress in cells by increasing the ratio of reduced to oxidized glutathione. After pretreatment with ROS scavengers for 1 h, cells were treated with **1** (10 μM) or **9** (20 μM) near their 4 h EC_{50} values, incubated for 1 h, and were treated with light (t_{irr} = 15 min, λ_{irr} = 460–470 nm, 170 J/cm^2) or were left in the dark. Viability was determined by the MTT assay 4 h after irradiation was complete. Data for cells treated with light are shown in Figure 9; cells treated showed minimal evidence of toxicity (viabilities > 90%). All four ROS scavengers provided significant levels of rescue in MDA-MB-231 cells treated with **1** and light (Figure 9A). Cells pretreated with the $^1O_2$ scavengers sodium azide and histidine showed viabilities near 100%, indicating nearly full rescue, which strongly suggests that Type II photosensitization ($^1O_2$) plays a crucial role in the cell death mechanism. In addition, cells treated with **1** showed a lesser, but statistically significant ($p < 0.01$) level of rescue (~20%) with D-Mannitol, a hydroxyl radical scavenger, which implicates hydroxyl radical and Type I photosensitization in cell death by **1**. Pretreatment with NAC also provided a strong rescue of cells treated by **1** and light that reached a level above 100% relative to cells treated with vehicle, light and no ROS scavenger. These data indicate that blocking of oxidative stress, presumably by increasing the ratio of reduced to oxidized glutathione in the cells, is enough to counteract the

photochemical generation of ROS by **1**. Levels of viability greater than 100% can be observed by MTT due to increased activity of oxidoreductases that drive reduction of MTT using NADH, whose concentration in cells is sensitive to the amount of reduced glutathione present.[99] In contrast with data for **1**, where large levels of rescue by ROS scavengers was observed, MDA-MB-231 cells treated with **9** (20 μM) underwent smaller (<30%), but statistically significant ($p < 0.01$) levels of rescue with sodium azide, histidine and NAC (Figure 9B). These data are consistent with Type II photosensitization being partially responsible for necrotic cell death. Cells pretreated with D-Mannitol showed no rescue vs. control cells treated with **9**, light and no scavenger, which rules out Type I photosensitization. Overall, complex **1** caused death at lower concentrations with higher phototherapeutic indexes than **9**, and several types of ROS ($^1O_2$, hydroxyl radical) were implicated in necrotic cell death.

A

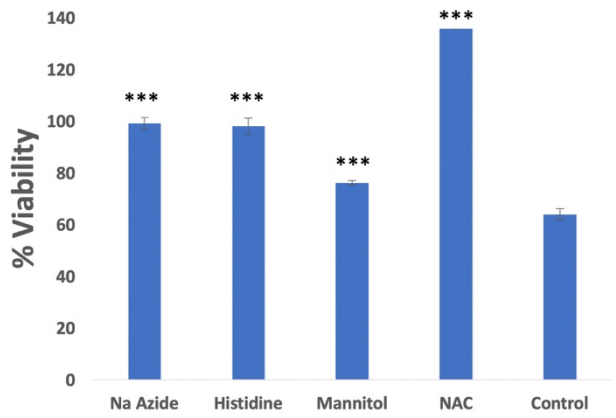

B

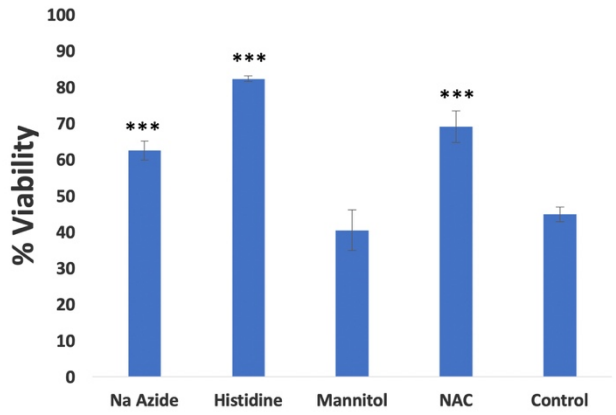

Figure 9. Cell viabilities of MDA-MB-231 determined 4 h after light treatment by MTT upon treatment with ROS scavengers NaN_3 (50 mM), mannitol (50 mM), histidine (50 mM), and N-acetylcysteine (5 mM) and either vehicle or A) **1** (10 μM) B) **9** (20 μM). Cells were incubated with ROS scavenger for 1 h before light treatment (t_{irr} = 15 min, λ_{irr} = 460–470 nm, 170 J/cm^2). Data are representative of three independent experiments; error bars are standard deviations of quadruplicate samples. *** $p<0.01$ and relates cells treated with no scavenger (control) to cells treated with ROS scavenger.

Conclusions

In conclusion, we report the synthesis, photochemical and biological characterization of a novel series of Ru(II) complexes that contain π-expansive ligands and a dual action PCT/PDT mode of action. A late-stage synthetic method was developed to introduce flanking aryl groups onto the dppn π-system that blocks the ability of resultant Ru(II) complexes to intercalate in DNA and enhances lipophilicity. However, introduction of the aryl substituents does not strongly influence the spectral or photophysical properties of the Ru(II) complexes vs. the parent derivative **1**. Despite the fact that **8**–**10** are not intercalators, the complexes associate with DNA in an electrostatic manner. Quantum yields for dissociations of monodentate pyridines by **8**–**10** were ~3 times higher than **1** and quantum yields for singlet oxygen generation were ~10% lower. Higher quantum efficiencies for photoactivated ligand dissociation observed for **8**–**10** vs. **1** makes these complexes attractive for PCT applications. The overall similarity of spectral and photophysical properties of **1** and **8**–**10** is likely due to the presence of minimal overlap between the π-system of the dppn ligand and the 10- and 15-aryl substituents, which is enforced by a crowded steric environment. Biological evaluation of **1** and **8**–**10** in breast and prostate cancer cells indicated that the preventing intercalation did not abolish bioactivity. Complexes **8**–**10** showed photoactivated death in both cell lines, although EC_{50} values were higher and photochemotherapeutic indexes were lower than data observed for **1**. Collectively these data indicate that intercalation is not necessary to achieve bioactivity, although it may enhance cell killing. In all cases cytotoxicity was promoted by ROS, particularly $^1O_2$. Investigations into the timescale and mechanism of cell death by **1** and **8**–**10** defined necrosis, rather than apoptosis as the mechanism of cell death that occurs

as early as 4 h after treatment with compounds and light. Importantly, cell death by necrosis can overcome resistance to apoptotic agents[100] and promote anti-tumor immunity.[101-104]

Acknowledgements

We gratefully acknowledge the National Institutes of Health (EB 016072), National Science Foundation (CHE 1800395) and Wayne State University for support of this research. For instrumentation support we thank the Hütteman laboratory, NSF (0840413) and Penrose Therapeut$_x$

Supporting Information

The following information is available free of charge on the internet:

Spectral data for **4**–**10**, DNA titration data for **9** and **10**, transient absorption spectra for **9** and **10**, DLS and time-resolved UV-vis data for **8**–**10**.

Synopsis: We report the synthesis, photochemical and biological characterization of a novel series of Ru(II) complexes that contain π-expansive ligands and a dual action PCT/PDT mode of action. These novel complexes are too bulky to undergo DNA intercalative. Nonetheless, tumor cell necrosis was observed in cells treated with the complexes and visible light only 4 h post treatment.

TOC Graphic

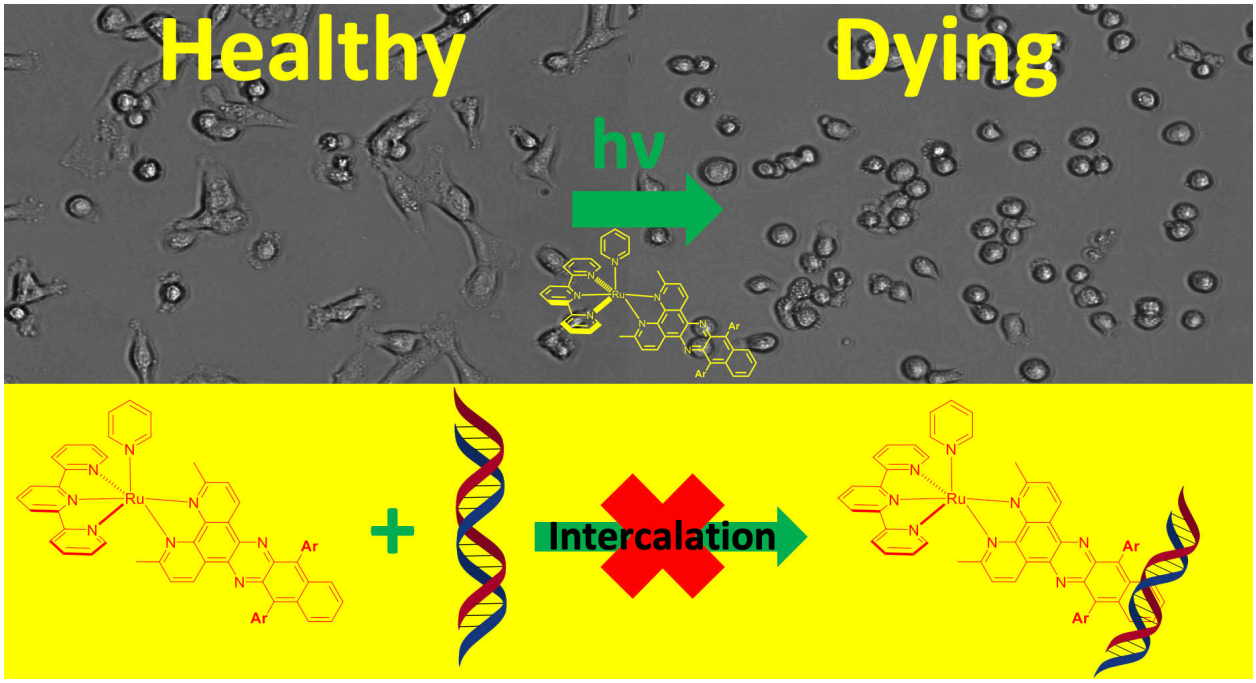

References

(1) Poynton, F. E.; Bright, S. A.; Blasco, S.; Williams, D. C.; Kelly, J. M.; Gunnlaugsson, T. *Chemical Society Reviews* **2017**, *46*, 7706-7756.

(2) White, J. K.; Schmehl, R. H.; Turro, C. *Inorg. Chim. Acta* **2017**, *454*, 7-20.

(3) Heinemann, F.; Karges, J.; Gasser, G. *Accounts of Chemical Research* **2017**, *50*, 2727-2736.

(4) Bonnet, S. *Dalton Trans.* **2018**, *47*, 10330-10343.

(5) Puckett, C. A.; Barton, J. K. *Biochemistry* **2008**, *47*, 11711-11716.

(6) Puckett, C. A.; Ernst, R. J.; Barton, J. K. *Dalton Trans.* **2010**, *39*, 1159-1170.

(7) Mulcahy, S. P.; Li, S.; Korn, R.; Xie, X.; Meggers, E. *Inorg. Chem.* **2008**, *47*, 5030-5032.

(8) Meggers, E. *Chem. Commun.* **2009**, 1001-1010.

(9) Respondek, T.; Sharma, R.; Herroon, M. K.; Garner, R. N.; Knoll, J. D.; Cueny, E.; Turro, C.; Podgorski, I.; Kodanko, J. J. *ChemMedChem* **2014**, *9*, 1306-1315.

(10) Ramalho, S. D.; Sharma, R.; White, J. K.; Aggarwal, N.; Chalasani, A.; Sameni, M.; Moin, K.; Vieira, P. C.; Turro, C.; Kodanko, J. J.; Sloane, B. F. *PLoS One* **2015**, *10*, e0142527/0142521-e0142527/0142517.

(11) Garner, R. N.; Gallucci, J. C.; Dunbar, K. R.; Turro, C. *Inorganic Chemistry* **2011**, *50*, 9213-9215.

(12) Respondek, T.; Garner, R. N.; Herroon, M. K.; Podgorski, I.; Turro, C.; Kodanko, J. J. *Journal of the American Chemical Society* **2011**, *133*, 17164-17167.

(13) Sears, R. B.; Joyce, L. E.; Ojaimi, M.; Gallucci, J. C.; Thummel, R. P.; Turro, C. *J. Inorg. Biochem.* **2013**, *121*, 77-87.

(14) Knoll, J. D.; Albani, B. A.; Durr, C. B.; Turro, C. *J. Phys. Chem. A* **2014**, *118*, 10603-10610.

(15) Knoll, J. D.; Albani, B. A.; Turro, C. *Acc. Chem. Res.* **2015**, *48*, 2280-2287.

(16) Wachter, E.; Heidary, D. K.; Howerton, B. S.; Parkin, S.; Glazer, E. C. *Chem. Commun.* **2012**, *48*, 9649-9651.

(17) Havrylyuk, D.; Deshpande, M.; Parkin, S.; Glazer, E. C. *Chem. Commun.* **2018**, *54*, 12487-12490.

(18) Bahreman, A.; Limburg, B.; Siegler, M. A.; Bouwman, E.; Bonnet, S. *Inorg. Chem.* **2013**, *52*, 9456-9469.

(19) Lameijer, L. N.; Ernst, D.; Hopkins, S. L.; Meijer, M. S.; Askes, S. H. C.; Le Devedec, S. E.; Bonnet, S. *Angew. Chem., Int. Ed.* **2017**, *56*, 11549-11553.

(20) Yin, H.; Stephenson, M.; Gibson, J.; Sampson, E.; Shi, G.; Sainuddin, T.; Monro, S.; McFarland, S. A. *Inorg. Chem.* **2014**, *53*, 4548-4559.

(21) Sainuddin, T.; McCain, J.; Pinto, M.; Yin, H.; Gibson, J.; Hetu, M.; McFarland, S. A. *Inorg. Chem.* **2016**, *55*, 83-95.

(22) Wang, L.; Yin, H.; Jabed, M. A.; Hetu, M.; Wang, C.; Monro, S.; Zhu, X.; Kilina, S.; McFarland, S. A.; Sun, W. *Inorg. Chem.* **2017**, *56*, 3245-3259.

(23) Ghosh, G.; Colon, K. L.; Fuller, A.; Sainuddin, T.; Bradner, E.; McCain, J.; Monro, S. M. A.; Yin, H.; Hetu, M. W.; Cameron, C. G.; McFarland, S. A. *Inorg. Chem.* **2018**, *57*, 7694-7712.

(24) Smithen, D. A.; Yin, H.; Beh, M. H. R.; Hetu, M.; Cameron, T. S.; McFarland, S. A.; Thompson, A. *Inorganic Chemistry* **2017**, *56*, 4121-4132.

(25) Monro, S.; Colon, K. L.; Yin, H.; Roque, J.; Konda, P.; Gujar, S.; Thummel, R. P.; Lilge, L.; Cameron, C. G.; McFarland, S. A. *Chem. Rev.* **2019**, *119*, 797-828.

(26) Damrauer, N. H.; Cerullo, G.; Yeh, A.; Boussie, T. R.; Shank, C. V.; McCusker, J. K. *Science* **1997**, *275*, 54.

(27) Knoll, J. D.; Albani, B. A.; Turro, C. *Chem. Commun.* **2015**, *51*, 8777-8780.

(28) Castano, A. P.; Demidova, T. N.; Hamblin, M. R. *Photodiagn. Photodyn. Ther.* **2005**, *1*, 279-293.

(29) Farrer, N. J.; Sadler, P. J. *Australian Journal of Chemistry* **2008**, *61*, 669-674.

(30) Arora, K.; Herroon, M.; Al-Afyouni, M. H.; Toupin, N. P.; Rohrabaugh, T. N.; Loftus, L. M.; Podgorski, I.; Turro, C.; Kodanko, J. J. *J. Am. Chem. Soc.* **2018**, *140*, 14367-14380.

(31) Pena, B.; Leed, N. A.; Dunbar, K. R.; Turro, C. *Journal of Physical Chemistry C* **2012**, *116*, 22186-22195.

(32) Xu, W.; Wittich, F.; Banks, N.; Zink, J.; Demas, J. N.; DeGraff, B. A. *Appl. Spectrosc.* **2007**, *61*, 1238-1245.

(33) Sgambellone, M. A.; David, A.; Garner, R. N.; Dunbar, K. R.; Turro, C. *J. Am. Chem. Soc.* **2013**, *135*, 11274-11282.

(34) Pena, B.; David, A.; Pavani, C.; Baptista, M. S.; Pellois, J.-P.; Turro, C.; Dunbar, K. R. *Organometallics* **2014**, *33*, 1100-1103.

(35) Lameijer Lucien, N.; Hopkins Samantha, L.; Brevé Tobias, G.; Askes Sven, H. C.; Bonnet, S. *Chemistry – A European Journal* **2016**, *22*, 18484-18491.

(36) Vidhisha, S.; Reddy, K. L.; Kumar, Y. P.; Srijana, M.; Satyanarayana, S. *Int. J. Pharm. Sci. Rev. Res.* **2014**, *25*, 197-205, 199 pp.

(37) Lei, W.; Zhou, Q.; Jiang, G.; Zhang, B.; Wang, X. *Photochem. Photobiol. Sci.* **2011**, *10*, 887-890.

(38) Liu, Y.; Hammitt, R.; Lutterman, D. A.; Joyce, L. E.; Thummel, R. P.; Turro, C. *Inorganic Chemistry* **2009**, *48*, 375-385.

(39) Zhao, R.; Hammitt, R.; Thummel, R. P.; Liu, Y.; Turro, C.; Snapka, R. M. *Dalton Trans.* **2009**, *251*, 10926-10931.

(40) Sun, Y.; El Ojaimi, M.; Hammitt, R.; Thummel, R. P.; Turro, C. *J. Phys. Chem. B* **2010**, *114*, 14664-14670.

(41) Loftus, L. M.; White, J. K.; Albani, B. A.; Kohler, L.; Kodanko, J. J.; Thummel, R. P.; Dunbar, K. R.; Turro, C. *Chemistry - A European Journal* **2016**, *22*, 3704-3708.

(42) Obare, S. O.; Murphy, C. J. *Inorg. Chem.* **2001**, *40*, 6080-6082.

(43) McConnell, A. J.; Lim, M. H.; Olmon, E. D.; Song, H.; Dervan, E. E.; Barton, J. K. *Inorg. Chem.* **2012**, *51*, 12511-12520.

(44) Monti, F.; Hahn, U.; Pavoni, E.; Delavaux-Nicot, B.; Nierengarten, J. F.; Armaroli, N. *Polyhedron* **2014**, *82*, 122-131.

(45) Foxon, S. P.; Green, C.; Walker, M. G.; Wragg, A.; Adams, H.; Weinstein, J. A.; Parker, S. C.; Meijer, A. J. H. M.; Thomas, J. A. *Inorg. Chem.* **2012**, *51*, 463-471.

(46) Chesneau, B.; Hardouin-Lerouge, M.; Hudhomme, P. *Org. Lett.* **2010**, *12*, 4868-4871.

(47) Gao, F.; Chen, X.; Wang, J.-Q.; Chen, Y.; Chao, H.; Ji, L.-N. *Inorg. Chem.* **2009**, *48*, 5599-5601.

(48) Chang, D. M.; Kim, Y. S. *J. Nanosci. Nanotechnol.* **2012**, *12*, 5709-5712.

(49) Shilpa, M.; Nagababu, P.; Kumar, Y. P.; Latha, J. N. L.; Reddy, M. R.; Karthikeyan, K. S.; Gabra, N.; Satyanarayana, S. *Journal of Fluorescence* **2011**, *21*, 1155-1164.

(50) Zhou, Q.-X.; Lei, W.-H.; Chen, J.-R.; Li, C.; Hou, Y.-J.; Wang, X.-S.; Zhang, B.-W. *Chemistry - A European Journal* **2010**, *16*, 3157-3165, S3157/3151-S3157/3111.

(51) Sun, Y.; Joyce, L. E.; Dickson, N. M.; Turro, C. *Chem. Commun.* **2010**, *46*, 2426-2428.

(52) Chen, Y.; Lei, W.; Jiang, G.; Zhou, Q.; Hou, Y.; Li, C.; Zhang, B.; Wang, X. *Dalton Trans.* **2013**, *42*, 5924-5931.

(53) Ardhammar, M.; Lincoln, P.; Norden, B. *J. Phys. Chem. B* **2001**, *105*, 11363-11368.

(54) Schatzschneider, U.; Niesel, J.; Ott, I.; Gust, R.; Alborzinia, H.; Woelfl, S. *ChemMedChem* **2008**, *3*, 1104-1109.

(55) Montalti, M.; Credi, A.; Prodi, L.; Gandolfi, M. T. *Handbook of Photochemistry*; 3rd ed.; CRC Press: Boca Raton, FL, 2006.

(56) Rohrabaugh, T. N., Jr.; Collins, K. A.; Xue, C.; White, J. K.; Kodanko, J. J.; Turro, C. *Dalton Trans.* **2018**, Ahead of Print.

(57) Nair, R. B.; Teng, E. S.; Kirkland, S. L.; Murphy, C. J. *Inorg. Chem.* **1998**, *37*, 139-141.

(58) Angeles-Boza, A. M.; Bradley, P. M.; Fu, P. K. L.; Wicke, S. E.; Bacsa, J.; Dunbar, K. R.; Turro, C. *Inorganic Chemistry* **2004**, *43*, 8510-8519.

(59) Chaires, J. B.; Dattagupta, N.; Crothers, D. M. *Biochemistry* **1982**, *21*, 3933-3940.

(60) Jiang, Y.; Chen, C.-F. *Synlett* **2010**, 1679-1681.

(61) Tena, A.; Vazquez-Guillo, R.; Marcos-Fernandez, A.; Hernandez, A.; Mallavia, R. *RSC Advances* **2015**, *5*, 41497-41505.

(62) Wei, P.; Duan, L.; Zhang, D.; Qiao, J.; Wang, L.; Wang, R.; Dong, G.; Qiu, Y. *J. Mater. Chem.* **2008**, *18*, 806-818.

(63) Deslandes, S.; Galaup, C.; Poole, R.; Mestre-Voegtle, B.; Soldevila, S.; Leygue, N.; Bazin, H.; Lamarque, L.; Picard, C. *Organic & Biomolecular Chemistry* **2012**, *10*, 8509-8523.

(64) Liu, Y.; Chouai, A.; Degtyareva, N. N.; Lutterman, D. A.; Dunbar, K. R.; Turro, C. *Journal of the American Chemical Society* **2005**, *127*, 10796-10797.

(65) Sun, Y.; Lutterman, D. A.; Turro, C. *Inorg. Chem.* **2008**, *47*, 6427-6434.

(66) Sun, Y.; Joyce, L. E.; Dickson, N. M.; Turro, C. *Chem. Commun.* **2010**, *46*, 6759-6761.

(67) Oenfelt, B.; Olofsson, J.; Lincoln, P.; Norden, B. *J. Phys. Chem. A* **2003**, *107*, 1000-1009.

(68) Brennaman, M. K.; Alstrum-Acevedo, J. H.; Fleming, C. N.; Jang, P.; Meyer, T. J.; Papanikolas, J. M. *J. Am. Chem. Soc.* **2002**, *124*, 15094-15098.

(69) Brennaman, M. K.; Meyer, T. J.; Papanikolas, J. M. *J. Phys. Chem. A* **2004**, *108*, 9938-9944.

(70) Albani, B. A.; Pena, B.; Leed, N. A.; de Paula, N. A. B. G.; Pavani, C.; Baptista, M. S.; Dunbar, K. R.; Turro, C. *J. Am. Chem. Soc.* **2014**, *136*, 17095-17101.

(71) Liu, Y.; Hammitt, R.; Lutterman, D. A.; Thummel, R. P.; Turro, C. *Inorganic Chemistry* **2007**, *46*, 6011-6021.

(72) Long, E. C.; Barton, J. K. *Acc. Chem. Res.* **1990**, *23*, 271-273.

(73) Foxon, S. P.; Metcalfe, C.; Adams, H.; Webb, M.; Thomas, J. A. *Inorg. Chem.* **2007**, *46*, 409-416.

(74) Neyhart, G. A.; Grover, N.; Smith, S. R.; Kalsbeck, W. A.; Fairley, T. A.; Cory, M.; Thorp, H. H. *J. Am. Chem. Soc.* **1993**, *115*, 4423-4428.

(75) Chouai, A.; Wicke, S. E.; Turro, C.; Bacsa, J.; Dunbar, K. R.; Wang, D.; Thummel, R. P. *Inorganic Chemistry* **2005**, *44*, 5996-6003.

(76) Suh, D.; Oh, Y.-K.; Chaires, J. B. *Process Biochem.* **2002**, *37*, 521-525.

(77) Kumar, C. V.; Barton, J. K.; Turro, N. J. *J. Am. Chem. Soc.* **1985**, *107*, 5518-5523.

(78) Velozo-Sa, V. S.; Pereira, L. R.; Lima, A. P.; Mello-Andrade, F.; Rezende, M. R. M.; Goveia, R. M.; Pires, W. C.; Silva, M. M.; Oliveira, K. M.; Ferreira, A. G.; Ellena, J.; Deflon, V. M.; Grisolia, C. K.; Batista, A. A.; Silveira-Lacerda, E. P. *Dalton Trans.* **2019**, *48*, 6026-6039.

(79) Silva, S. L. R.; Baliza, I. R. S.; Dias, R. B.; Sales, C. B. S.; Gurgel Rocha, C. A.; Soares, M. B. P.; Correa, R. S.; Batista, A. A.; Bezerra, D. P. *Scientific Reports* **2019**, *9*, 1-11.

(80) Ravi, C.; Vuradi, R. K.; Avudoddi, S.; Yata, P. K.; Putta, V. R.; Srinivas, G.; Merugu, R.; Satyanarayana, S. *Nucleosides, Nucleotides Nucleic Acids* **2019**, *38*, 788-806.

(81) Kralj, J.; Bolje, A.; Polancec, D. S.; Steiner, I.; Grzan, T.; Tupek, A.; Stojanovic, N.; Hohloch, S.; Urankar, D.; Osmak, M.; Sarkar, B.; Brozovic, A.; Kosmrlj, J. *Organometallics* **2019**, Ahead of Print.

(82) Bhatti, M. Z.; Ali, A.; Duong, H.-Q.; Chen, J.; Rahman, F.-U. *J. Inorg. Biochem.* **2019**, *194*, 52-64.

(83) Acharya, S.; Maji, M.; Purkait, K.; Mukherjee, A.; Ruturaj; Gupta, A.; Mukherjee, A. *Inorg. Chem.* **2019**, *58*, 9213-9224.

(84) Tadic, A.; Poljarevic, J.; Krstic, M.; Kajzerberger, M.; Arandjelovic, S.; Radulovic, S.; Kakoulidou, C.; Papadopoulos, A. N.; Psomas, G.; Grguric-Sipka, S. *New J. Chem.* **2018**, *42*, 3001-3019.

(85) Mohan, N.; Mohamed Subarkhan, M. K.; Ramesh, R. *J. Organomet. Chem.* **2018**, *859*, 124-131.

(86) Adeyemo, A. A.; Shettar, A.; Bhat, I. A.; Kondaiah, P.; Mukherjee, P. S. *Dalton Trans.* **2018**, *47*, 8466-8475.

(87) Mello-Andrade, F.; da Costa, W. L.; Pires, W. C.; Pereira, F. d. C.; Cardoso, C. G.; Lino-Junior, R. d. S.; Irusta, V. R. C.; Carneiro, C. C.; de Melo-Reis, P. R.; Castro, C. H.; Almeida, M. A. P.; Batista, A. A.; Silveira-Lacerda, E. d. P. *Tumor Biol.* **2017**, *39*, 1010428317695933/1010428317695931-1010428317695933/1010428317695933.

(88) Khamrang, T.; Kartikeyan, R.; Velusamy, M.; Rajendiran, V.; Dhivya, R.; Perumalsamy, B.; Akbarsha, M. A.; Palaniandavar, M. *RSC Advances* **2016**, *6*, 114143-114158.

(89) Huang, H.; Zhang, P.; Chen, Y.; Qiu, K.; Jin, C.; Ji, L.; Chao, H. *Dalton Trans.* **2016**, *45*, 13135-13145.

(90) Wang, Y.-C.; Qian, C.; Peng, Z.-L.; Hou, X.-J.; Wang, L.-L.; Chao, H.; Ji, L.-N. *J. Inorg. Biochem.* **2014**, *130*, 15-27.

(91) Hayward, R. L.; Schornagel, Q. C.; Tente, R.; Macpherson, J. S.; Aird, R. E.; Guichard, S.; Habtemariam, A.; Sadler, P.; Jodrell, D. I. *Cancer Chemother. Pharmacol.* **2005**, *55*, 577-583.

(92) Gaiddon, C.; Jeannequin, P.; Bischoff, P.; Pfeffer, M.; Sirlin, C.; Loeffler, J. P. *J. Pharmacol. Exp. Ther.* **2005**, *315*, 1403-1411.

(93) Berghe, T. V.; Vanlangenakker, N.; Parthoens, E.; Deckers, W.; Devos, M.; Festjens, N.; Guerin, C. J.; Brunk, U. T.; Declercq, W.; Vandenabeele, P. *Cell Death And Differentiation* **2009**, *17*, 922.

(94) Rieger, A. M.; Nelson, K. L.; Konowalchuk, J. D.; Barreda, D. R. *J. Visualized Exp.* **2011**, 2597, 2594 pp.

(95) Ishow, E.; Gourdon, A.; Launay, J.-P. *Chem. Commun. (Cambridge)* **1998**, 1909-1910.

(96) Jiang, C. W.; Chao, H.; Li, R. H.; Li, H.; Ji, L. N. *Polyhedron* **2001**, *20*, 2187-2193.

(97) Dong, S.; Hwang, H.-M.; Shi, X.; Holloway, L.; Yu, H. *Chem. Res. Toxicol.* **2000**, *13*, 585-593.

(98) Aruoma, O. I.; Halliwell, B.; Hoey, B. M.; Butler, J. *Free Radical Biol. Med.* **1989**, *6*, 593-597.

(99) Stepanenko, A. A.; Dmitrenko, V. V. *Gene* **2015**, *574*, 193-203.

(100) Su, Z.; Yang, Z.; Xie, L.; DeWitt, J. P.; Chen, Y. *Cell Death Differ.* **2016**, *23*, 748-756.

(101) Rajendrakumar, S. K.; Uthaman, S.; Cho, C.-S.; Park, I.-K. *Biomacromolecules* **2018**, *19*, 1869-1887.

(102) Zitvogel, L.; Casares, N.; Pequignot, M. O.; Chaput, N.; Albert, M. L.; Kroemer, G. *Adv. Immunol.* **2004**, *84*, 131-179.

(103) Melcher, A.; Gough, M.; Todryk, S.; Vile, R. *J. Mol. Med.* **1999**, *77*, 824-833.

(104) Curtin, J. F.; Liu, N.; Candolfi, M.; Xiong, W.; Assi, H.; Yagiz, K.; Edwards, M. R.; Michelsen, K. S.; Kroeger, K. M.; Liu, C.; Muhammad, G. A. K. M.; Clark, M. C.; Arditi, M.; Comin-Anduix, B.; Ribas, A.; Lowenstein, P. R.; Castro, M. G. *PLoS Med.* **2009**, *6*, 0083-0100.

Synopsis: We report the synthesis, photochemical and biological characterization of a novel series of Ru(II) complexes that contain π-expansive ligands and a dual action PCT/PDT mode of action. These novel complexes are too bulky to undergo DNA intercalative. Nonetheless, tumor cell necrosis was observed in cells treated with the complexes and visible light only 4 h post treatment.

TOC Graphic